CHAPTER 3

OFFSET MODULATION

3.1 INTRODUCTION

In Chapter 2 the draw backs associated with the various methods in the PAPR field were discussed. Ideally a method which requires low implementation complexity and does not lead to a severe BER degradation, as the number of carriers increases, is desired. It should also not require any additional bandwidth expansion or the transmission of any side information to reconstruct the original message signal. This chapter begins by introducing a novel method called offset modulation, which meets a number of these requirements.

3.2 OFFSET MODULATION

Consider the discrete complex output of an N-point inverse fast Fourier transformed OFDM signal, given by

$$m_n = \frac{1}{\sqrt{N}} \sum_{k=0}^{N-1} X_k e^{j\frac{2\pi nk}{N}}, \qquad n = 0, 1, ..., N-1 \tag{3.1}$$

$$= \frac{1}{\sqrt{N}} \sum_{k=0}^{N-1} (a_k + jb_k) \cdot \left(\cos\left(\frac{2\pi nk}{N}\right) + j \sin\left(\frac{2\pi nk}{N}\right) \right). \tag{3.2}$$

In Eq (3.1), X_k represents the complex signal output $(a_k + jb_k)$ of the IFFT. This signal may be modulated using the method which follows.

$$\Phi_{1n} = \frac{\Re(m_n)}{\varsigma} = \frac{1}{\varsigma\sqrt{N}} \sum_{k=0}^{N-1} \left(a_k \cos\left(\frac{2\pi nk}{N}\right) - b_k \sin\left(\frac{2\pi nk}{N}\right) \right) \quad \text{and} \tag{3.3}$$

$$\Phi_{2n} = \frac{\Im(m_n)}{\varsigma} = \frac{1}{\varsigma\sqrt{N}} \sum_{k=0}^{N-1} \left(b_k \cos\left(\frac{2\pi nk}{N}\right) + a_k \sin\left(\frac{2\pi nk}{N}\right) \right). \tag{3.4}$$

Here $\Re$ and $\Im$ refer to the real and imaginary parts of the OFDM message signal, ς refers to a constant division term, whereas Φ_{1n} and Φ_{2n} represent the equivalent real and imaginary OFDM phase mapping. These discrete Φ_{1n} and Φ_{2n} terms are passed through a DAC and are now combined into a unique co-sinusoid

$$\cos(2\pi f_c t + \Phi_1(t) + \Psi_{os}) - \cos(2\pi f_c t + \Phi_2(t)). \tag{3.5}$$

After utilising the following identity [91]

$$\cos(z_1) - \cos(z_2) = 2\sin\left(\frac{z_2 - z_1}{2}\right) \cdot \sin\left(\frac{z_1 + z_2}{2}\right) \tag{3.6}$$

thereafter, Eq (3.5) can be written as

$$2\sin\left(\frac{\Phi_2(t) - \Phi_1(t) - \Psi_{os}}{2}\right) \cdot \sin\left(2\pi f_c t + \frac{\Phi_1(t) + \Psi_{os} + \Phi_2(t)}{2}\right) \tag{3.7}$$

where, Ψ_{os} refers to an offset term, $\Phi_1(t)$ and $\Phi_2(t)$ represent the equivalent real and imaginary OFDM phase mapping. In this type of modulation the parameters (Ψ_{os}, ς) are chosen such that $\Psi_{os} >> \Phi_2(t) - \Phi_1(t)$. This implies that the Ψ_{os} term will dominate the expression, hence the name offset modulation (OM-OFDM) [92, 93] is proposed to describe this operation. A block diagram, depicted in Fig. 3.1, shows the processes involved during an OM-OFDM transmission. In Appendix A a more detailed description of the OM modulator and OM demodulator structure is presented. The proposed OM-OFDM process, depicted in Fig. 3.1, still maintains the fundamental OFDM building blocks. During an OM-OFDM transmission, depicted in Fig. 3.1, binary input data are mapped to complex symbols. Pilot symbols are thereafter inserted between these complex symbols.

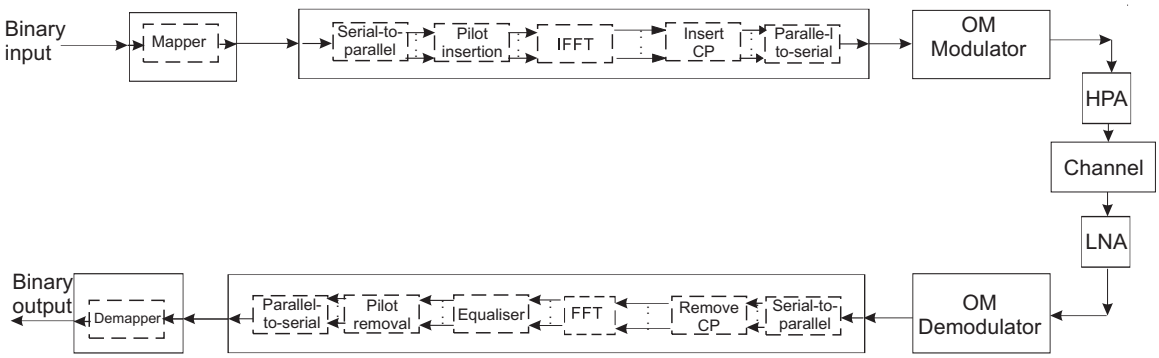

Figure 3.1: Transmitter receiver structure

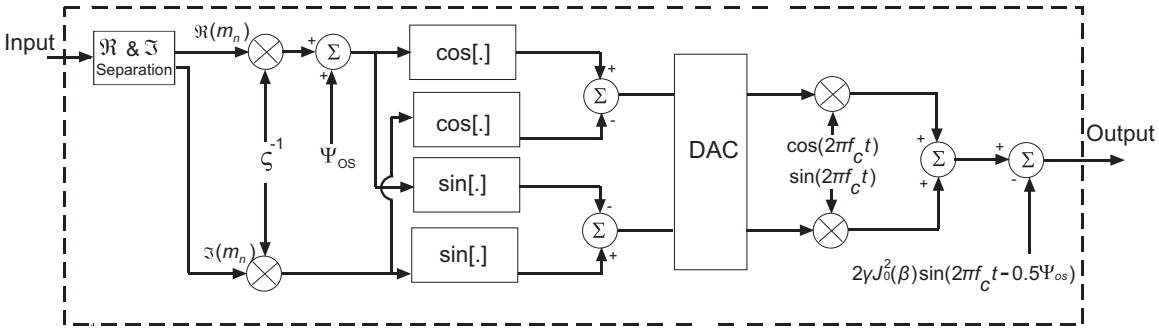

Figure 3.2: OM modulator structure

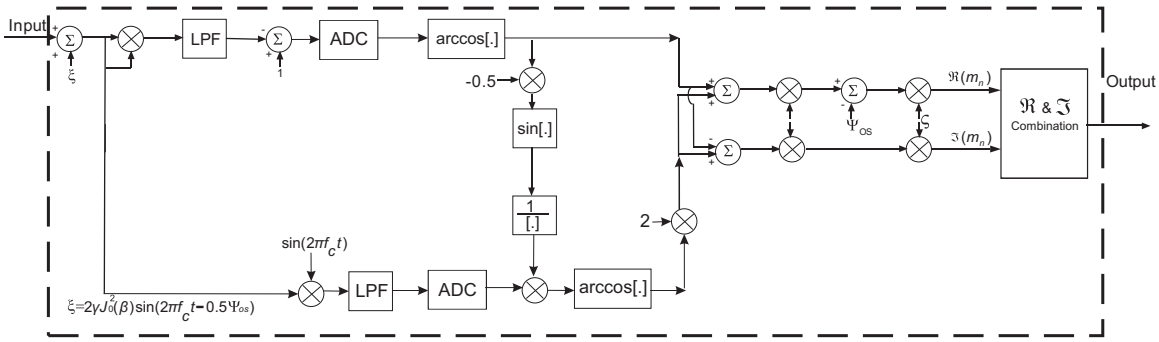

Figure 3.3: OM demodulator structure

The subsequent signal is passed through an IFFT; thereafter a cyclic pre-fix is appended to the signal. This process is identical to that previously seen in an OFDM transmission. The difference between an OFDM and OM-OFDM transmission lies in the modulation process. The OM modulator structure in an OM-OFDM transmission is used to reduce the PAPR of the OFDM transmission. The OM modulator structure receives a complex OFDM input and after various steps, depicted in Fig 3.2 and discussed in Appendix A, outputs

an OM-OFDM signal. This subsequent signal is passed through a HPA and transmitted across a channel. This process produces a spectrally efficient signal illustrated in Fig. 3.4, when compared to a classical OFDM transmission. The OM-OFDM transmission contains

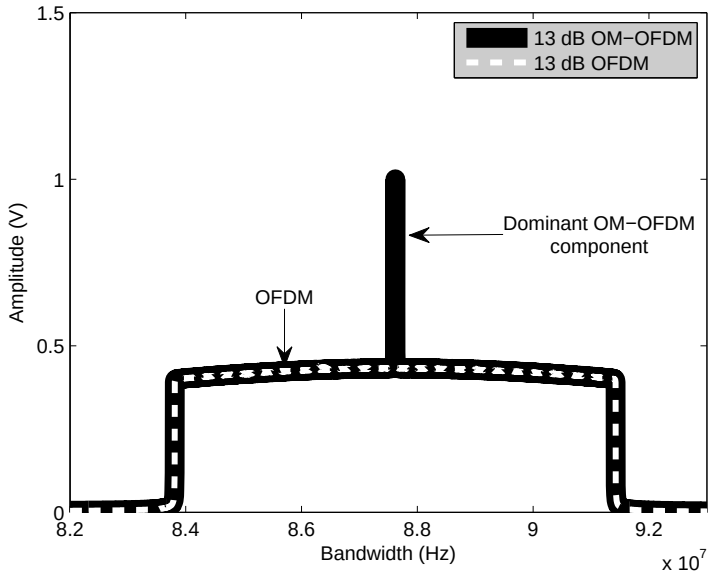

Figure 3.4: An averaged normalised bandwidth occupancy comparison between OM-OFDM and OFDM with identical throughput when, using a 64-QAM 8 k mode of the DVB - T2 standard.

a dominant component; as the dominant component becomes prominent, the PAPR of the signal decreases. However, in reality some energy restrictions are imposed on a transmitter, thus the other components can contain less energy, leading to a BER trade-off.

The received signal, depicted in Fig. 3.1, is passed through a LNA. This is followed by an OM demodulator, depicted in Fig 3.3, which receives the modulated signal and outputs a complex OFDM signal. The cyclic prefix is thereafter removed. The purpose of this CP, as previously discussed, is to mitigate some of the effects of the channel. Thereafter, an FFT is performed on the signal, in order to recover the original message signal.

The transmission may appear to be a phase modulated signal, therefore losing its attractive OFDM properties. However, the OM-OFDM system's transmitter receiver structure (Fig. 3.1.) maintains the fundamental OFDM building blocks. Thus, the OM-OFDM

equalisation process is identical to that employed in OFDM. Channel state information (CSI) is extracted from the pilot symbols and used during the equalisation process to mitigate the effects of fading. Thus, OM-OFDM maintains the ease of OFDM equalisation. The pilot symbols are thereafter removed and the complex symbols are de-mapped to binary output data.

3.3 BANDWIDTH OCCUPANCY OF OFFSET MODULATION

In this section the bandwidth occupancy of an OM-OFDM transmission may be investigated by considering a discrete complex OFDM signal

$$m_n = \frac{1}{\sqrt{N}} \sum_{k=0}^{N-1} X_k e^{j\frac{2\pi nk}{N}} = \frac{1}{\sqrt{N}} \sum_{k=0}^{N-1} X_k e^{jw_n k} \tag{3.8}$$

where w_n is an arbitrary chosen variable used to simplify the analysis, Eq (3.8) may also be written as

$$m_n = \frac{1}{\sqrt{N}} \sum_{k=0}^{N-1} (a_k + jb_k)(\cos(w_n k) + j\sin(w_n k)) \tag{3.9}$$

and it can then be shown that

$$\Phi_{1n} = \frac{\Re[m_n]}{\varsigma} \approx \sum_{k=0}^{N-1} \beta_1 \cos(w_n k) - \beta_2 \sin(w_n k) \tag{3.10}$$

$$\Phi_{2n} = \frac{\Im[m_n]}{\varsigma} \approx \sum_{k=0}^{N-1} \beta_2 \cos(w_n k) + \beta_1 \sin(w_n k). \tag{3.11}$$

where Φ_{1n} and Φ_{2n} are the equivalent real and imaginary discrete OFDM phase mapping, β_1 and β_2 are mean values defined as the adapted real and imaginary phase deviation of an OM-OFDM signal respectively. The approximation sign introduced in Eq (3.10) and Eq (3.11) is due to the fact that the β_1 and β_2 terms are message-dependent. An attempt is made to characterise the deviation of a message by the introduction of mean value terms, hence the introduction of the approximation. After incorporating this into the unique co-

sinusoidal (Eq (3.5)), the following expression is obtained

$$u_n \approx \Re\left[e^{j(2\pi f_c n+\Psi_{os}+\sum_{k=0}^{N-1}\beta_1\cos(w_n k)-\beta_2\sin(w_n k))}\right]-\Re\left[e^{j(2\pi f_c n+\sum_{k=0}^{N-1}\beta_2\cos(w_n k)+\beta_1\sin(w_n k))}\right], \tag{3.12}$$

in Eq (3.12), u_n is the discrete signal which is to be transmitted. With the aid of Bessel functions [94], the Fourier series can be written as

$$e^{j(\beta\sin(w_n k))}=\sum_{l=-\infty}^{\infty}J_l(\beta)e^{j(lw_n k)} \quad \text{and} \quad e^{j(\beta\cos(w_n k))}=\sum_{m=-\infty}^{\infty}J_m(\beta)e^{j(mw_n k+\frac{m\pi}{2})}. \tag{3.13}$$

In Eq (3.13), $J_l(\beta)$ and $J_m(\beta)$ are Bessel functions of the first kind of order l and m respectively with argument β. After substituting Eq (3.13) into Eq (3.12), it can then be shown that

$$\begin{aligned} u_n \approx \prod_{k=0}^{N-1}\Bigg(\Bigg[\sum_{l=-\infty}^{\infty}\sum_{m=-\infty}^{\infty}J_m(\beta_1)J_l(\beta_2)\cos\left(\frac{2\pi nk}{N}(f_c+l+m)+\Psi_{os}+\frac{m\pi}{2}\right)\Bigg] \\ -\Bigg[\sum_{l=-\infty}^{\infty}\sum_{m=-\infty}^{\infty}J_m(\beta_2)J_l(\beta_1)\cdot\cos\left(\frac{2\pi nk}{N}(f_c+l+m)+\frac{m\pi}{2}\right)\Bigg]\Bigg). \end{aligned} \tag{3.14}$$

Here, f_c is the carrier frequency. Consider the case when $l=m=\pm1$, $N=1$ and after using the $J_{-n}(\beta)=(-1)^n J_n(\beta)$ relationship, the various amplitude and phase components obtained from Eq (3.14) are summarised in Table 3.1. Upon studying the positive $(l+m\geq 0)$ and

Table 3.1: Components of Eq (3.14) when $l=m=\pm1$ and $N=1$

l	m	l+m	$J_m(\beta_1)\cdot J_l(\beta_2)$	$J_l(\beta_1)\cdot J_m(\beta_2)$
-1	-1	-2	$-J_1(\beta_1)\cdot -J_1(\beta_2)$	$-J_1(\beta_1)\cdot -J_1(\beta_2)$
0	-1	-1	$-J_1(\beta_1)\cdot J_0(\beta_2)$	$J_0(\beta_1)\cdot -J_1(\beta_2)$
-1	0	-1	$J_0(\beta_1)\cdot -J_1(\beta_2)$	$-J_1(\beta_1)\cdot J_0(\beta_2)$
1	-1	0	$-J_1(\beta_1)\cdot J_1(\beta_2)$	$J_1(\beta_1)\cdot -J_1(\beta_2)$
0	0	0	$J_0(\beta_1)\cdot J_0(\beta_2)$	$J_0(\beta_1)\cdot J_0(\beta_2)$
-1	1	0	$J_1(\beta_1)\cdot -J_1(\beta_2)$	$-J_1(\beta_1)\cdot J_1(\beta_2)$
1	0	1	$J_0(\beta_1)\cdot J_1(\beta_2)$	$J_1(\beta_1)\cdot J_0(\beta_2)$
0	1	1	$J_1(\beta_1)\cdot J_0(\beta_2)$	$J_0(\beta_1)\cdot J_1(\beta_2)$
1	1	2	$J_1(\beta_1)\cdot J_1(\beta_2)$	$J_1(\beta_1)\cdot J_1(\beta_2)$

negative $(l+m<0)$ frequency components of Table 3.1, in conjunction with various other

($l = m = \pm 1, \pm 2 \ldots$ and $N = 1$) bandwidth occupancy cases, a particular relationship indicated by Eq (3.15) emerges

$$u_n = \sum_{y=0}^{2x} \left| \sum_{z=0}^{2x-y} 2\sin\left(\frac{\pi(2x-2z-y) \pm 2\Psi_{os}}{4}\right) \cdot J_{|-x+z|}(\beta_1) \left(\frac{|-x+z+\frac{1}{2}|}{-x+z+\frac{1}{2}}\right)^{|-x+z|} \cdot J_{|x-y-z|}(\beta_2) \left(\frac{|x-y-z+\frac{1}{2}|}{x-y-z+\frac{1}{2}}\right)^{|x-y-z|} \cdot \sin\left(2\pi(f_c + y f_d) + \frac{2\Psi_{os} \pm y\pi}{4}\right) \right|. \quad (3.15)$$

In Eq (3.15), f_d is an integer multiple of the modulation frequency and $2x$ refers to an even number of frequency components of interest. In order to demonstrate the relationship between Eq (3.14) and Eq (3.15), consider the case when $l + m = 2$ and $y = 2$. After using Table 3.1 ($l + m = 2$) obtained from Eq (3.14), for this case it can be shown that

$$\begin{aligned} & J_1(\beta_1) \cdot J_1(\beta_2) \cdot \left(\cos\left(2\pi(f_c + 2f_d) + \Psi_{os} + \frac{\pi}{2}\right) - \cos\left(2\pi(f_c + 2f_d) + \frac{\pi}{2}\right) \right) \\ = \; & 2J_1(\beta_1) \cdot J_1(\beta_2) \cdot \left(\sin\left(\frac{\Psi_{os}}{2}\right) \cdot \sin\left(2\pi(f_c + 2f_d) + \frac{\Psi_{os}}{2} + \frac{\pi}{2}\right) \right). \end{aligned} \quad (3.16)$$

Substituting $2x = 2$ and $y = 2$ into Eq (3.15), results in

$$\begin{aligned} & 2\sin\left(\frac{2\Psi_{os}}{4}\right) \cdot J_1(\beta_1) \left(\frac{|-\frac{1}{2}|}{-\frac{1}{2}}\right) \cdot J_1(\beta_2) \left(\frac{|-\frac{1}{2}|}{-\frac{1}{2}}\right) \cdot \sin\left(2\pi(f_c + 2f_d) + \frac{2\Psi_{os} + 3\pi}{4}\right) \\ = \; & 2J_1(\beta_1) J_1(\beta_2) \sin\left(\frac{\Psi_{os}}{2}\right) \cdot \sin\left(2\pi(f_c + 2f_d) + \frac{\Psi_{os}}{2} + \frac{\pi}{2}\right). \end{aligned} \quad (3.17)$$

This result correlates with that from Eq (3.16), thus validating some of the components of Eq (3.15) with those in Eq (3.14). In a similar manner, all of the other components can be validated. In most cases, the adapted phase deviation (β_1 and β_2) of the signal is not known beforehand; however, a reasonably good approximation can be made, based on

$$\alpha_1 \approx E[max(|\Re(m(t))|)], \quad (3.18)$$

$$\alpha_2 \approx E[max(|\Im(m(t))|)], \quad (3.19)$$

$$\beta_1 \approx \frac{\alpha_1}{\varsigma} \quad \text{and} \quad (3.20)$$

$$\beta_2 \approx \frac{\alpha_2}{\varsigma}. \quad (3.21)$$

In Eq (3.18), Eq (3.19), Eq (3.20) and Eq (3.21), α_1 and α_2, refer to the real and imaginary phase deviations of the OFDM signal respectively and E [.] is the expected value. Typically, there is no interest in all the frequency components, but rather in the more dominant components. Hence, the bandwidth can be defined by considering only those sidebands which contain significant power. Suppose, for explanation purposes, the first two components ($2x = 2$) are of interest and $\beta \approx \beta_1 \approx \beta_2$. After inspecting Eq (3.15), Fig. 3.5 depicts the frequency spectrum and its corresponding amplitude components. This frequency spectrum is different from that of a conventional phase modulated signal.

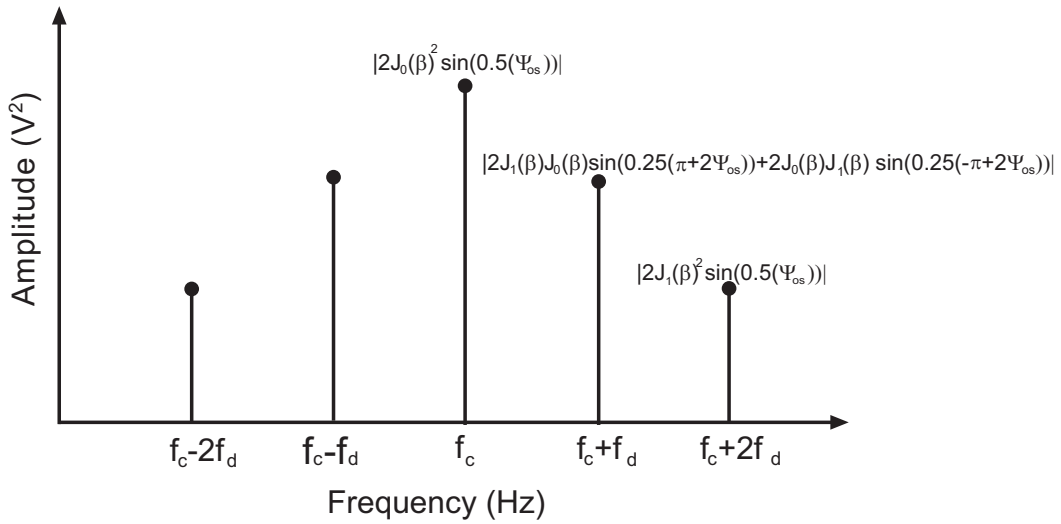

Figure 3.5: Theoretically derived (Eq (3.15)) frequency spectrum of an OM-OFDM signal.

The squaring of the Bessel functions limits the bandwidth occupancy of the signal. If β is sufficiently small ($\beta = 0.02$), it can be seen that a large percentage of the power is constrained within these ($2x = 2$) frequency components. This depiction may serve as a simplistic OM-OFDM bandwidth occupancy description. The dominant frequency component is given by $2J_0(\beta)^2 \sin(2\pi f_c t - \frac{\Psi_{os}}{2})$, provided $\Psi_{os} >> \Phi_2(t) - \Phi_1(t)$. In such a case, the dominant frequency component can be shown to be dependent on the Ψ_{os} term.

This expression also provides some insight into an OM-OFDM transmission, namely the bandwidth expansion is dependent on the ς term. The higher the ς term, the lower the phase β, thus indicating less bandwidth expansion. Ideally an attempt might be made to choose ς as high as possible. However, as the ς term increases, the signal would lose

resolution and this would lead to an increase in the BER. Thus far it has been shown that the dominant frequency component of an OM-OFDM transmission can be predicted by $2J_0(\beta)^2\sin(2\pi f_c t - \frac{\Psi_{os}}{2})$. By subtracting $2\gamma J_0(\beta)^2\sin(2\pi f_c t - \frac{\Psi_{os}}{2}), \quad 0 \leq \gamma < 1$, (where γ is the dominant frequency component control factor) from the dominant frequency component at the transmitter (Fig. 3.2) and re-instating the subtracted term at the receiver (Fig. 3.3), the PAPR may be controlled.

The receiver gains knowledge of the subtracted term by examining the PAPR of the incoming signal, from which the Ψ_{os}, ς and γ terms can be extracted by using a simple look-up table. Since the Ψ_{os} and ς terms are in most cases identical, only the γ term is subsequently extracted from the received signal's PAPR. It might be argued that after a transmission through a multi-path fading channel, the received and transmitted PAPR might differ. However, for an n-tap channel, each path affects both the RMS and peak value of the received signal equally. Therefore the PAPR from each path is equivalent to the originally sent PAPR.

This principle can be demonstrated by using the 8k mode of the DVB-T2 standard [95] to transmit 64-QAM OM-OFDM data through a 5-tap typical-urban area [96] at a low 10 dB SNR (E_b/N_o). The complementary cumulative distribution function (CCDF) of such a transmission, depicted in Fig. 3.6, indicates that the sent and received PAPRs are almost identical. In the next section, the manner in which the dominant frequency component is varied and the resultant BER characteristics are presented.

3.4 SYMBOL AND BIT ERROR RATE CHARACTERISTICS OF OFFSET MODULATION

A received signal under AWGN conditions is expressed as [87, 97]

$$r(t) = u(t) + n(t) = u(t) + N_c(t)\cos(2\pi f_c t) - N_s(t)\sin(2\pi f_c t). \tag{3.22}$$

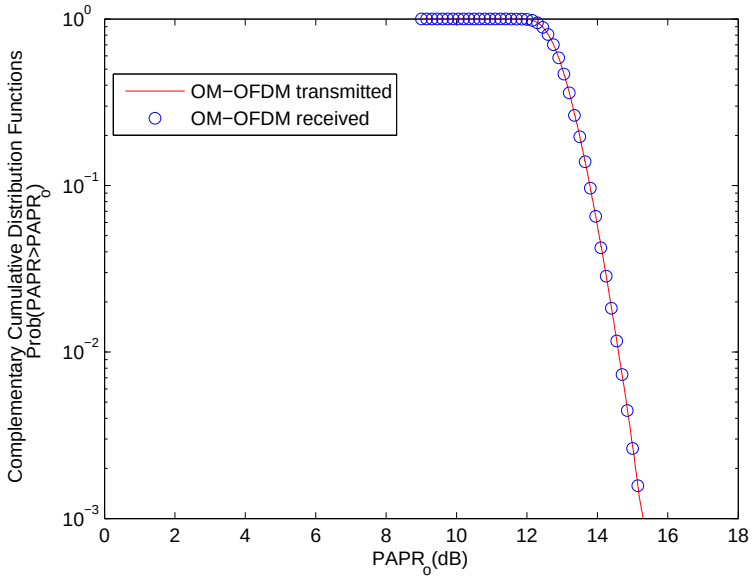

Figure 3.6: Complementary cumulative distribution functions for a 64-QAM constellation, when using the DVB-T2 standard for a 5-tap typical urban area channel at a 10 dB signal-to-noise ratio (E_b/N_o).

In Eq (3.22), $u(t)$ refers to an offset-modulated signal and $n(t)$ represents AWGN. The $N_c(t)$ and $N_s(t)$ expressions refer to the in-phase and the quadrature components of noise respectively. The noise expression can also be written as

$$\begin{aligned} n(t) &= \sqrt{N_c^2(t)+N_s^2(t)}\sin\left(2\pi f_c t + arctan\frac{N_c(t)}{N_s(t)}\right) \\ &= V_n(t)\sin(2\pi f_c t+\Phi_n(t)). \end{aligned} \tag{3.23}$$

In Eq (3.23), $V_n(t)$ and $\Phi_n(t)$ represent the envelope and phase of the band-pass noise. The offset modulated signal $u(t)$ can be expressed as

$$\begin{aligned} u(t) &= 2\sin\left(\frac{\Phi_2(t)-\Phi_1(t)-\Psi_{os}}{2}\right)\cdot\sin\left(2\pi f_c t+\frac{\Phi_1(t)+\Psi_{os}+\Phi_2(t)}{2}\right) \\ &\approx A_c(t)\sin(2\pi f_c t+\Phi(t)), \end{aligned} \tag{3.24}$$

where $A_c(t)$ and $\Phi(t)$ can be seen as the envelope and phase of an offset modulated signal. After using phasor manipulation, depicted in Fig. 3.7, it can be shown that the received signal

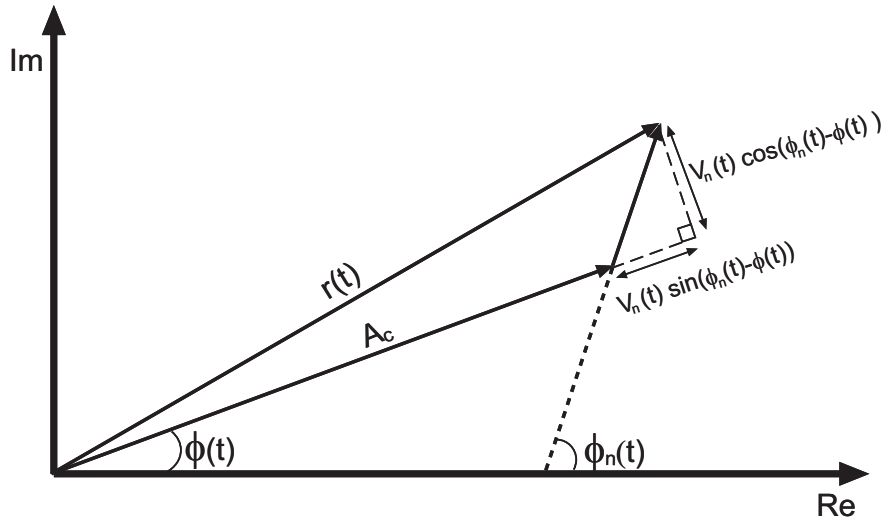

Figure 3.7: OM-OFDM phasor [97]

can be written as

$$\begin{aligned} r(t) &= (A_c(t) + V_n(t)\sin(\Phi_n(t) - \Phi(t))) \cdot \\ &\quad \sin\left(2\pi f_c t + \Phi(t) + arctan\left[\frac{V_n(t)\cos(\Phi_n(t) - \Phi(t))}{A_c + V_n(t)\cos(\Phi_n(t) - \Phi(t))}\right]\right). \end{aligned} \tag{3.25}$$

If the assumption is made that the signal is much larger than the noise, in this case

$$r(t) \approx (A_c(t) + V_n(t)\sin(\Phi_n(t) - \Phi(t))) \cdot \sin\left(2\pi f_c t + \Phi(t) + \frac{V_n(t)\cos(\Phi_n(t) - \Phi(t))}{A_c}\right) \tag{3.26}$$

it can be seen from Eq (3.26), that the noise expression at the y branch of the demodulator can be written as

$$Y_n(t) = \frac{V_n(t)\cos(\Phi_n(t) - \Phi(t))}{A_c}. \tag{3.27}$$

By applying the following identity,

$$\cos(\alpha - \beta) = \cos\alpha\cos\beta + \sin\alpha\sin\beta, \tag{3.28}$$

the noise expression can be represented by

$$Y_n(t) = \frac{V_n(t)\cos(\Phi_n(t))\cos(\Phi(t)) + V_n(t)\sin(\Phi_n(t))\sin(\Phi(t))}{A_c} \tag{3.29}$$

therefore

$$Y_n(t) = \frac{n_c(t)\cos(\Phi(t)) + n_s\sin(\Phi(t))}{A_c}. \tag{3.30}$$

In Eq (3.30), n_c and n_s refer to the noise co-sinusoidal and sinusoidal expressions, respectively. An auto correlation is performed on the noise, in order to study the spectrum characteristics of this expression. This can be expressed as

$$\begin{aligned} E[Y_n(t)Y_n(t+\tau)] = E\Bigg[& \frac{n_c(t)n_c(t+\tau)\cos(\Phi(t))\cos(\Phi(t+\tau))}{{A_c}^2} + \\ & \frac{n_c(t)n_s(t+\tau)\cos(\Phi(t))\sin(\Phi(t+\tau))}{{A_c}^2} + \\ & \frac{n_s(t)n_c(t+\tau)\sin(\Phi(t))\cos(\Phi(t+\tau))}{{A_c}^2} + \\ & \frac{n_s(t)n_s(t+\tau)\sin(\Phi(t))\sin(\Phi(t+\tau))}{{A_c}^2}\Bigg]. \end{aligned} \tag{3.31}$$

According to [97], for stationary white symmetric noise

$$n_c(t)n_s(t+\tau) = n_c(t)n_s(t+\tau) = 0 \tag{3.32}$$

$$R_{nc}(\tau) = n_c(t)n_c(t+\tau) \tag{3.33}$$

$$R_{ns}(\tau) = n_s(t)n_s(t+\tau) \tag{3.34}$$

$$R_{ns}(\tau) = R_{nc}(\tau) \tag{3.35}$$

where $R_{nc}(\tau)$ and $R_{ns}(\tau)$ are band-pass signals. Substituting Eq (3.32), Eq (3.33), Eq (3.34) and Eq (3.35) into Eq (3.31), results in the following expression

$$E[Y_n(t)Y_n(t+\tau)] = E\left[\frac{R_{nc}(\tau)\cos(\Phi(t))\cos(\Phi(t+\tau))}{{A_c}^2} + \frac{R_{ns}(\tau)\sin(\Phi(t))\sin(\Phi(t+\tau))}{{A_c}^2}\right]. \tag{3.36}$$

After using the identity presented in Eq (3.28) in conjunction with Eq (3.35), Eq (3.36) simplifies to

$$E[Y_n(t)Y_n(t+\tau)] = \frac{R_{nc}(\tau)}{{A_c}^2}E[\cos(\Phi(t+\tau)-\Phi(t))]. \tag{3.37}$$

According to [97], at any fixed time t, a random variable $Z(t,\tau)=\Phi(t+\tau)-\Phi(t)$ is the difference between two jointly Gaussian random variables. This is itself a Gaussian random variable with mean equal to zero and a variance given by

$$\begin{aligned} {\sigma_Z}^2 &= E[(\Phi(t+\tau)-\Phi(t))^2] \\ &= E[\Phi^2(t+\tau)]+E[\Phi^2(t)]-2R_\Phi(\tau) \\ &= 2(R_\Phi(0)-R_\Phi(\tau)), \end{aligned} \tag{3.38}$$

where, as previously mentioned, $2R_\Phi(\tau)$ is a band-pass signal. Substituting Eq (3.38) into Eq (3.37) results in

$$\begin{aligned} E[Y_n(t)Y_n(t+\tau)] &= \frac{R_{nc}(\tau)}{{A_c}^2}E[\cos(\Phi(t+\tau)-\Phi(t))] \\ &= \frac{R_{nc}(\tau)}{{A_c}^2}\Re\left(E\left[e^{j(\Phi(t+\tau)-\Phi(t))}\right]\right) \\ &= \frac{R_{nc}(\tau)}{{A_c}^2}\Re\left(E\left[e^{j(Z(t,\tau))}\right]\right) \\ &= \frac{R_{nc}(\tau)}{{A_c}^2}\Re\left(e^{-\left(\frac{{\sigma_Z}^2}{2}\right)}\right) \\ &= \frac{R_{nc}(\tau)}{{A_c}^2}\Re\left(e^{-(R_\Phi(0)-R_\Phi(\tau))}\right) \\ &= \frac{R_{nc}(\tau)}{{A_c}^2}\left(e^{-(R_\Phi(0)-R_\Phi(\tau))}\right). \end{aligned} \tag{3.39}$$

From the autocorrelation of the noise, the power spectral density of the noise can be written as

$$\begin{aligned} S_Y(f) &= \mathscr{F}[R_Y(\tau)] \\ &= \mathscr{F}\left[\frac{R_{nc}(\tau)}{{A_c}^2}\left(e^{-(R_\Phi(0)-R_\Phi(\tau))}\right)\right] \end{aligned}$$

$$\begin{aligned} &= \frac{e^{-R_\Phi(0)}}{A_c^2}\mathscr{F}\left[R_{nc}(\tau)e^{R_\Phi(\tau)}\right] \\ &= \frac{e^{-R_\Phi(0)}}{A_c^2}\mathscr{F}\left[R_{nc}(\tau)g(\tau)\right] \\ &= \frac{e^{-R_\Phi(0)}}{A_c^2}S_{nc}(f)\star G(f), \end{aligned} \tag{3.40}$$

where $G(f)$ is the Fourier transform ($\mathscr{F}$) of $g(\tau) = e^{R_\Phi(\tau)}$, $S_{nc}(f)$ is the Fourier transform of R_{nc} and the $\star$ refers to a convolutional process. Now suppose the discussion is confined to a specific bandwidth of $-\frac{B_c}{2}$ to $\frac{B_c}{2}$. For this case suppose, $S_{nc}(f) = N_o$, here N_o is the power spectral density of the additive noise. The power spectral density may now be expressed as

$$\begin{aligned} S_Y(f) &= \frac{e^{-R_\Phi(0)}}{A_c^2}N_o\int_{-\frac{B_c}{2}}^{\frac{B_c}{2}} G(f)\,df \\ &\approx \frac{e^{-R_\Phi(0)}}{A_c^2}N_o\int_{-\infty}^{\infty} G(f)\,df \\ &= \frac{e^{-R_\Phi(0)}}{A_c^2}N_o g(\tau)\Big|_{\tau=0} \\ &= \frac{e^{-R_\Phi(0)}}{A_c^2}N_o e^{R_\Phi(0)} \\ &= \frac{N_o}{A_c^2}. \end{aligned} \tag{3.41}$$

Suppose $A_c \approx 2\ \sin\left(\frac{-\varphi}{2}\right)$ (from Eq (3.24)) where φ refers to a constant term. With the use of Eq (3.41) and by following a similar methodology, the Y and X output power-spectral density of the noise component can be shown to be written as

$$S_Y(f) \approx \frac{N_o}{4\sin^2\left(\frac{-\varphi}{2}\right)} \tag{3.42}$$

and

$$S_X(f) \approx N_o. \tag{3.43}$$

After band limiting (B_c) the transmission ($0 > B > \frac{B_c}{2}$), the noise variance at the output of the various branches of the demodulator (Fig. 3.1) is given by

$$\sigma_Y^2 \approx \frac{N_o}{8\sin^2\left(\frac{-\varphi}{2}\right)} \quad \text{and} \quad \sigma_X^2 \approx \frac{N_o}{2} \tag{3.44}$$

where, by inspection, φ may be approximated by Table 3.2. In Table 3.2, γ is the dominant

Table 3.2: Selection of a φ term, based on γ and α

	$0 < \alpha < 0.1$	$0.1 \leq \alpha < 0.2$	$0.2 \leq \alpha < 0.3$
$\varphi \approx \frac{\beta\sin(\Psi_{os})}{4(1-\gamma)}$	$0 \leq \gamma < 0.988$	$0 \leq \gamma < 0.97$	$0 \leq \gamma < 0.96$
$\varphi \approx \frac{\beta\sin(\Psi_{os})}{5(1-\gamma)}$	$0.988 \leq \gamma < 1$	$0.97 \leq \gamma < 1$	$0.96 \leq \gamma < 1$

frequency component control factor and the α ($\alpha \approx \alpha_1 \approx \alpha_2$) and β ($\beta \approx \beta_1 \approx \beta_2$) terms originate from Eq (3.18), Eq (3.19), Eq (3.20) and Eq (3.21). The proposed φ term is obtained, based on a number of observations, provided $0 \leq \varphi \leq \frac{\pi}{2}$, namely

$$N_o \propto \frac{1}{\sin(\Psi_{os})} \tag{3.45}$$

$$N_o \propto \varsigma \tag{3.46}$$

$$N_o \propto [1-\gamma]. \tag{3.47}$$

From these observations the φ term in Table 3.2 is proposed. Therefore, from the γ and α term of a particular transmission (shown in Table 3.2), either the

$$\varphi \approx \frac{\beta\sin(\Psi_{os})}{4(1-\gamma)} \quad \text{or} \tag{3.48}$$

$$\varphi \approx \frac{\beta\sin(\Psi_{os})}{5(1-\gamma)} \tag{3.49}$$

term, can be used to describe the noise properties. In the sub-sections which follow the BER and symbol error rate (SER) expression for an OM-OFDM transmission will be derived by using the noise variance expression (Eq (3.44)).

3.4.1 A 4-PAM symbol and bit error rate derivation

Consider a 4-PAM baseband signal, depicted in Fig. 3.8, with signal points $s_0 = -3d\sqrt{\frac{\xi_s}{\xi_{av}}}$, $s_1 = -d\sqrt{\frac{\xi_s}{\xi_{av}}}$, $s_2 = d\sqrt{\frac{\xi_s}{\xi_{av}}}$ and $s_3 = 3d\sqrt{\frac{\xi_s}{\xi_{av}}}$, where d is the Euclidean distance, ξ_s is the energy per symbol and ξ_{av} is the average energy per symbol. Suppose the received signal at

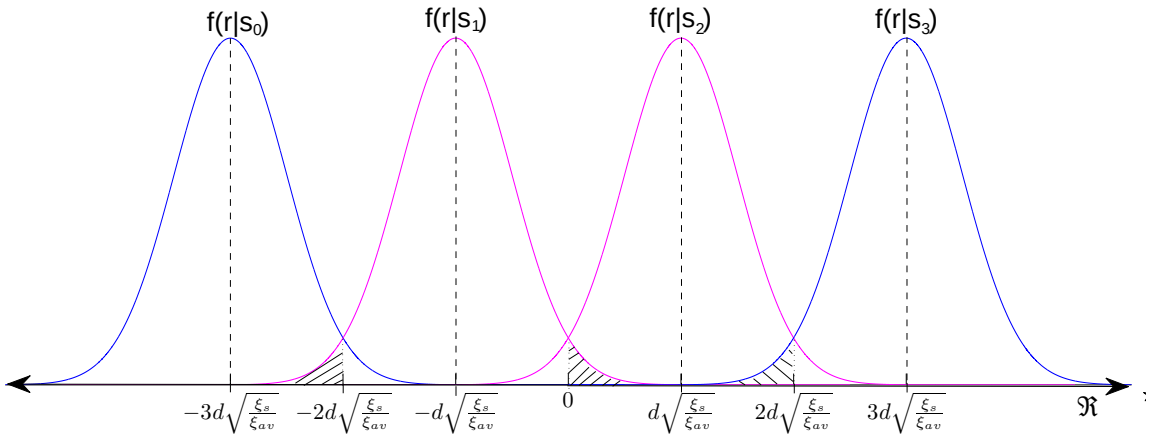

Figure 3.8: Conditional PDFs of four signals

the output of the demodulator is

$$r = s_3 + n = 3d\sqrt{\frac{\xi_s}{\xi_{av}}} + n. \tag{3.50}$$

In Eq (3.50), n represents AWGN. The decision rule compares the received signal (r) with a threshold. If $r > 2d\sqrt{\frac{\xi_s}{\xi_{av}}}$, a decision is made in favour of s_3, if $r < 2d\sqrt{\frac{\xi_s}{\xi_{av}}}$, the decision is made in favour of s_2. The conditional probability density functions for r are

$$\begin{aligned} f(r|s_0) &= \frac{1}{\sqrt{2\pi}\sigma} e^{\frac{-\left(r+3d\sqrt{\frac{\xi_s}{\xi_{av}}}\right)^2}{2\sigma^2}} \\ f(r|s_1) &= \frac{1}{\sqrt{2\pi}\sigma} e^{\frac{-\left(r+d\sqrt{\frac{\xi_s}{\xi_{av}}}\right)^2}{2\sigma^2}} \\ f(r|s_2) &= \frac{1}{\sqrt{2\pi}\sigma} e^{\frac{-\left(r-d\sqrt{\frac{\xi_s}{\xi_{av}}}\right)^2}{2\sigma^2}} \end{aligned}$$

$$f(r|s_3) = \frac{1}{\sqrt{2\pi}\sigma} e^{\frac{-\left(r-3d\sqrt{\frac{\xi_s}{\xi_{av}}}\right)^2}{2\sigma^2}} \tag{3.51}$$

where σ is the variance of the noise. Given that s_3 was transmitted, the probability of a symbol error is

$$\begin{aligned} p(e|s_3) &= \int_{-\infty}^{2d\sqrt{\frac{\xi_s}{\xi_{av}}}} p(r|s_3) \quad dr \\ &= \frac{1}{\sqrt{2\pi}\sigma} \int_{-\infty}^{2d\sqrt{\frac{\xi_s}{\xi_{av}}}} e^{\frac{-\left(r-3d\sqrt{\frac{\xi_s}{\xi_{av}}}\right)^2}{2\sigma^2}} \quad dr \\ &= \frac{1}{\sqrt{\pi}} \int_{-\infty}^{-d\sqrt{\frac{\xi_s}{2\sigma^2\xi_{av}}}} e^{-t^2} \quad dt \\ &= \frac{1}{\sqrt{\pi}} \int_{d\sqrt{\frac{\xi_s}{2\sigma^2\xi_{av}}}}^{\infty} e^{-t^2} \quad dt \\ &= \frac{1}{2}\text{erfc}\left(d\sqrt{\frac{\xi_s}{2\sigma^2\xi_{av}}}\right) \end{aligned} \tag{3.52}$$

in Eq (3.52), erfc is the error function. It can similarly be shown that $p(e|s_0) = p(e|s_3) = \frac{1}{2}\text{erfc}\left(d\sqrt{\frac{\xi_s}{2\sigma^2\xi_{av}}}\right)$. Given that s_1 was transmitted, the probability of a symbol error is

$$\begin{aligned} p(e|s_1) &= \int_{-\infty}^{-2d\sqrt{\frac{\xi_s}{\xi_{av}}}} p(r|s_1)dr + \int_0^{\infty} p(r|s_1)dr \\ &= \frac{1}{\sqrt{2\pi}\sigma} \int_{-\infty}^{-2d\sqrt{\frac{\xi_s}{\xi_{av}}}} e^{\frac{-\left(r+d\sqrt{\frac{\xi_s}{\xi_{av}}}\right)^2}{2\sigma^2}} dr + \frac{1}{\sqrt{2\pi}\sigma} \int_0^{\infty} e^{\frac{-\left(r+d\sqrt{\frac{\xi_s}{\xi_{av}}}\right)^2}{2\sigma^2}} dr \\ &= \frac{1}{\sqrt{\pi}} \int_{-\infty}^{-d\sqrt{\frac{\xi_s}{2\sigma^2\xi_{av}}}} e^{-t^2} dt + \frac{1}{\sqrt{\pi}} \int_{d\sqrt{\frac{\xi_s}{2\sigma^2\xi_{av}}}}^{\infty} e^{-t^2} dt \\ &= \frac{1}{2}\text{erfc}\left(d\sqrt{\frac{\xi_s}{2\sigma^2\xi_{av}}}\right) + \frac{1}{2}\text{erfc}\left(d\sqrt{\frac{\xi_s}{2\sigma^2\xi_{av}}}\right) \\ &= \text{erfc}\left(d\sqrt{\frac{\xi_s}{2\sigma^2\xi_{av}}}\right). \end{aligned} \tag{3.53}$$

Similarly, it can be shown that $p(e|s_2) = p(e|s_1) = \text{erfc}\left(d\sqrt{\frac{\xi_s}{2\sigma^2\xi_{av}}}\right)$. The SER is then

$$P_{SER} = p(s_0)p(e|s_0) + p(s_1)p(e|s_1) + p(s_2)p(e|s_2) + p(s_3)p(e|s_3) \tag{3.54}$$

where $p(s_0)$, $p(s_1)$, $p(s_2)$ and $p(s_3)$ are the probabilities of the s_0, s_1, s_2 and s_3 symbols respectively. If it is assumed that each symbol is equally probable i.e. $p(s_0) = p(s_1) = p(s_2) = p(s_3) = \frac{1}{4}$, the SER for a 4-PAM constellation can be written as

$$\begin{aligned} SER_{4PAM} &= \frac{1}{4}\text{erfc}\left(d\sqrt{\frac{\xi_s}{2\sigma^2\xi_{av}}}\right) + \frac{2}{4}\text{erfc}\left(d\sqrt{\frac{\xi_s}{2\sigma^2\xi_{av}}}\right) \\ &= \frac{3}{4}\text{erfc}\left(d\sqrt{\frac{\xi_s}{2\sigma^2\xi_{av}}}\right). \end{aligned} \tag{3.55}$$

A particular symbol s_1 is comprised of a number of bits. The number of bits denoted by k is dependent on the constellation and can be written as $k = \log_2 M$. When the constellation is Gray-coded and $(p(s_0|s_1)|p(s_2|s_1)) >> p(s_3|s_1)$, the subsequent number of bits in error can be written as

$$BER_{4PAM} = \frac{3}{4k}\text{erfc}\left(d\sqrt{\frac{kE_b}{2\sigma^2\xi_{av}}}\right) \tag{3.56}$$

where E_b is the energy per bit and $\frac{\xi_s}{\sigma^2} = \frac{kE_b}{\sigma^2}$.

3.4.2 A 4-QAM symbol and bit error rate derivation

Similarly for a 4-QAM constellation, depicted in Fig. 3.9, the symbol s_1 is correctly detected only if r falls within the following region

$$p(c|s_1) = p\big(\Re_r > 0\big|s_1\big)\,p\big(\Im_r > 0\big|s_1\big). \tag{3.57}$$

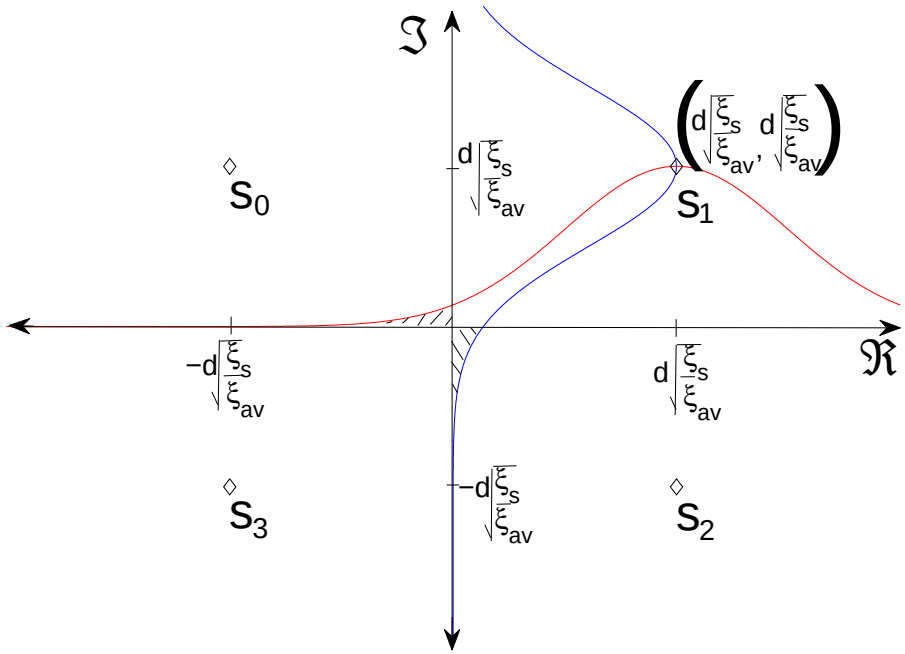

Figure 3.9: 4-QAM constellation

In Eq (3.57), $\Re_r$ and $\Im_r$ are the received real and imaginary components. The probability of the real component of r being greater than 0, given that s_1 was transmitted, is

$$\begin{aligned} p(\Re_r > 0|s_1) &= 1 - \frac{1}{\sqrt{2\pi}\sigma_x}\int_{-\infty}^{0} e^{\frac{-\left(\Re_r - d\sqrt{\frac{\xi_s}{\xi_{av}}}\right)^2}{2\sigma_x^2}} dr \\ &= 1 - \frac{1}{2}\text{erfc}\left(d\sqrt{\frac{\xi_s}{2\sigma_x^2\xi_{av}}}\right) \end{aligned} \tag{3.58}$$

where, σ_x is the variance of the x component of the noise. Similarly, the probability of the imaginary component of r being greater than 0, given that s_1 was transmitted, is

$$\begin{aligned} p(\Im_r > 0|s_1) &= 1 - \frac{1}{\sqrt{2\pi}\sigma_y}\int_{-\infty}^{0} e^{\frac{-\left(\Im_r - d\sqrt{\frac{\xi_s}{\xi_{av}}}\right)^2}{2\sigma_y^2}} dr \\ &= 1 - \frac{1}{2}\text{erfc}\left(d\sqrt{\frac{\xi_s}{2\sigma_y^2\xi_{av}}}\right). \end{aligned} \tag{3.59}$$

In Eq (3.59), σ_y is the variance of the y component of the noise. The probability of s_1 being detected correctly is

$$p(c|s_1) = \left[1-\frac{1}{2}\text{erfc}\left(d\sqrt{\frac{\xi_s}{2\sigma_x^2\xi_{av}}}\right)\right]\left[1-\frac{1}{2}\text{erfc}\left(d\sqrt{\frac{\xi_s}{2\sigma_y^2\xi_{av}}}\right)\right]. \quad (3.60)$$

As previously stated in Eq (3.44), for an OM-OFDM transmission

$$\sigma_X^2 \approx \frac{N_o}{2} \quad \text{and} \quad \sigma_Y^2 \approx \frac{N_o}{8\sin^2\left(\frac{-\varphi}{2}\right)} \quad (3.61)$$

after substituting Eq (3.61) into Eq (3.60), this results in

$$p(c|s_1) = \left[1-\frac{1}{2}\text{erfc}\left(d\sqrt{\frac{\xi_s}{N_0\xi_{av}}}\right)\right]\left[1-\frac{1}{2}\text{erfc}\left(d\sqrt{\frac{4\sin^2(-\frac{\varphi}{2})\xi_s}{\xi_{av}N_o}}\right)\right]. \quad (3.62)$$

Now let

$$p = \text{erfc}\left(d\sqrt{\frac{\xi_s}{\xi_{av}N_o}}\right) \quad \text{and} \quad l = \text{erfc}\left(d\sqrt{\frac{4\sin^2(-\frac{\varphi}{2})\xi_s}{\xi_{av}N_o}}\right). \quad (3.63)$$

The resultant probability of symbol s_1 being incorrectly detected is

$$\begin{aligned} p(e|s_1) &= 1-p(c|s_1) \\ &= 1-\left[1-\frac{p}{2}\right]\left[1-\frac{l}{2}\right] \\ &= \frac{2l+2p-p\cdot l}{4}. \end{aligned} \quad (3.64)$$

It can similarly be shown that $p(e|s_1) = p(e|s_2) = p(e|s_3) = p(e|s_0)$. The SER is then

$$P_{SER} = p(s_0)p(e|s_0)+p(s_1)p(e|s_1)+p(s_2)p(e|s_2)+p(s_3)p(e|s_3) \quad (3.65)$$

where $p(s_0)$, $p(s_1)$, $p(s_2)$ and $p(s_3)$ are the probabilities of the s_0, s_1, s_2 and s_3 symbols respectively. If it is assumed that each symbol is equally probable i.e. $p(s_0) = p(s_1) =$

$p(s_2) = p(s_3) = \frac{1}{4}$, then the symbol error probability for this 4-QAM constellation is

$$SER_{4QAM} = \frac{2l + 2p - p \cdot l}{4}. \tag{3.66}$$

If the particular constellation is Gray-coded and $(p(s_0|s_1) \mid p(s_2|s_1)) >> p(s_3|s_1)$ for this 4-QAM constellation, the subsequent bit error rate probability, when symbol s_1 is incorrectly detected, can be written as

$$p(e|b_1) = 1 - \left[1 - \frac{1}{2k}\text{erfc}\left(d\sqrt{\frac{kE_b}{\xi_{av}N_0}}\right)\right]\left[1 - \frac{1}{2k}\text{erfc}\left(d\sqrt{\frac{4k\sin^2(-\frac{\varphi}{2})E_b}{\xi_{av}N_o}}\right)\right] \tag{3.67}$$

where E_b is the energy per bit and $\frac{\xi_s}{N_0} = \frac{kE_b}{N_0}$. Now let

$$\wp = \text{erfc}\left(d\sqrt{\frac{kE_b}{\xi_{av}N_o}}\right) \tag{3.68}$$

and

$$\ell = \text{erfc}\left(d\sqrt{\frac{4k\sin^2(-\frac{\varphi}{2})E_b}{\xi_{av}N_o}}\right). \tag{3.69}$$

The subsequent bit error rate probability when symbol s_1 is incorrectly detected can be written as

$$\begin{aligned} p(e|b_1) &= 1 - \left[1 - \frac{\wp}{2k}\right]\left[1 - \frac{\ell}{2k}\right] \\ &= \frac{2k \cdot \ell + 2\wp \cdot k - \wp \cdot \ell}{4k^2}. \end{aligned} \tag{3.70}$$

It can similarly be shown that $p(e|b_1) = p(e|b_2) = p(e|b_3) = p(e|b_0)$. The BER for this 4-QAM constellation is

$$\begin{aligned} BER_{4QAM} &= p(s_0)p(e|b_0) + p(s_1)p(e|b_1) + p(s_2)p(e|b_2) + p(s_3)p(e|b_3) \\ &= \frac{2k \cdot \ell + 2\wp \cdot k - \wp \cdot \ell}{4k^2}. \end{aligned} \tag{3.71}$$

3.4.3 A 16-QAM symbol and bit error rate derivation

3.4.3.1 Symbols in the centre of a constellation

For a 16-QAM constellation, depicted in Fig. 3.10, the symbol s_5 is correctly detected only

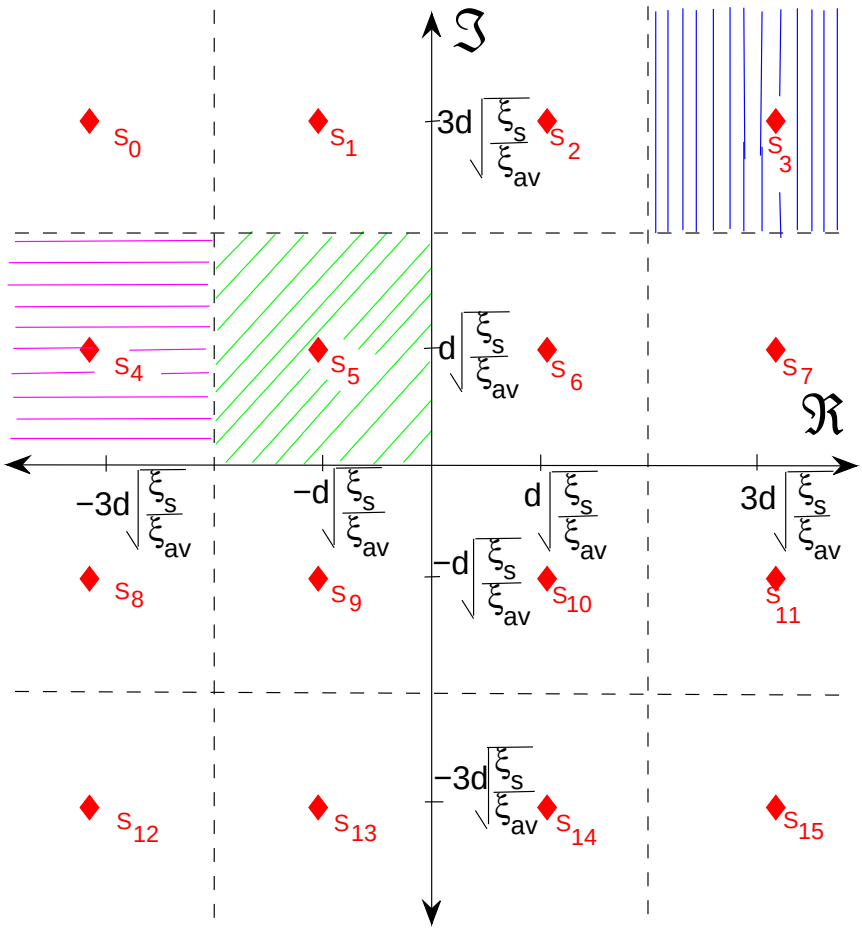

Figure 3.10: 16-QAM constellation

if r falls in the forward hashed green region as indicated by the following expression

$$p(c|s_5) = p\left(\Re_r \leq 0, \Re_r > -2d\sqrt{\frac{\xi_s}{\xi_{av}}}\middle| s_5\right) p\left(\Im_r > 0, \Im_r \leq 2d\sqrt{\frac{\xi_s}{\xi_{av}}}\middle| s_5\right). \quad (3.72)$$

By making use of Eq (3.53) for a 4-PAM constellation

$$p(c|s_5) = \left[1 - \text{erfc}\left(d\sqrt{\frac{\xi_s}{2\sigma_x^2\xi_{av}}}\right)\right]\left[1 - \text{erfc}\left(d\sqrt{\frac{\xi_s}{2\sigma_y^2\xi_{av}}}\right)\right]. \tag{3.73}$$

After substituting Eq (3.61) into Eq (3.73), this results in

$$p(c|s_5) = \left[1 - \text{erfc}\left(d\sqrt{\frac{\xi_s}{N_0\xi_{av}}}\right)\right]\left[1 - \text{erfc}\left(d\sqrt{\frac{4\sin^2(-\frac{\varphi}{2})\xi_s}{\xi_{av}N_o}}\right)\right]. \tag{3.74}$$

After substituting Eq (3.63) into Eq (3.74), the resultant probability of symbol s_5 being incorrectly detected is

$$\begin{aligned} p(e|s_5) &= 1 - p(c|s_5). \\ &= l + p - p \cdot l. \end{aligned} \tag{3.75}$$

In addition, it can be shown that $p(e|s_5) = p(e|s_6) = p(e|s_9) = p(e|s_{10})$. The subsequent bit error rate probability when symbol s_5 is incorrectly detected can be written as

$$\begin{aligned} p(e|b_5) &= 1 - \left[1 - \frac{1}{k}\text{erfc}\left(d\sqrt{\frac{kE_b}{\xi_{av}N_0}}\right)\right]\left[1 - \frac{1}{k}\text{erfc}\left(d\sqrt{\frac{4k\sin^2(-\frac{\varphi}{2})E_b}{\xi_{av}N_o}}\right)\right] \\ &= \frac{k\cdot\ell + \wp\cdot k - \wp\cdot\ell}{k^2}. \end{aligned} \tag{3.76}$$

Similarly it can be shown that $p(e|b_5) = p(e|b_6) = p(e|b_9) = p(e|b_{10})$.

3.4.3.2 Symbols in the corner of a constellation

In Fig. 3.10, the symbol s_3 is correctly detected only if r falls in the vertical blue region, as indicated by the following expression

$$p(c|s_3) = p\left(\Re_r > 2d\sqrt{\frac{\xi_s}{\xi_{av}}}\middle| s_3\right) p\left(\Im_r > 2d\sqrt{\frac{\xi_s}{\xi_{av}}}\middle| s_3\right). \tag{3.77}$$

By making use of Eq (3.60) for a 4-QAM constellation and Eq (3.61)

$$\begin{aligned} p(c|s_3) &= \left[1-\frac{1}{2}\text{erfc}\left(d\sqrt{\frac{\xi_s}{2\sigma_x^2\xi_{av}}}\right)\right]\left[1-\frac{1}{2}\text{erfc}\left(d\sqrt{\frac{\xi_s}{2\sigma_y^2\xi_{av}}}\right)\right] \\ &= \left[1-\frac{1}{2}\text{erfc}\left(d\sqrt{\frac{\xi_s}{N_0\xi_{av}}}\right)\right]\left[1-\frac{1}{2}\text{erfc}\left(d\sqrt{\frac{4\sin^2(-\frac{\varphi}{2})\xi_s}{\xi_{av}N_o}}\right)\right]. \end{aligned} \quad (3.78)$$

From Eq (3.63) the probability of symbol s_3 being detected incorrectly is

$$\begin{aligned} p(e|s_3) &= 1-p(c|s_3) \\ &= \frac{2l+2p-p\cdot l}{4}. \end{aligned} \quad (3.79)$$

It can also be shown that $p(e|s_3)=p(e|s_0)=p(e|s_{12})=p(e|s_{15})$. As previously mentioned, from Eq (3.68) and Eq (3.69), the subsequent bit error rate probability, when symbol s_3 is incorrectly detected, can be written as

$$\begin{aligned} p(e|b_3) &= 1-\left[1-\frac{1}{2k}\text{erfc}\left(d\sqrt{\frac{kE_b}{\xi_{av}N_0}}\right)\right]\left[1-\frac{1}{2k}\text{erfc}\left(d\sqrt{\frac{4k\sin^2(-\frac{\varphi}{2})E_b}{\xi_{av}N_o}}\right)\right] \\ &= \frac{2k\cdot\ell+2\wp\cdot k-\wp\cdot\ell}{4k^2}. \end{aligned} \quad (3.80)$$

Similarly it can be shown that $p(e|b_3)=p(e|b_0)=p(e|b_{12})=p(e|b_{15})$.

3.4.3.3 Symbols at the edge of a constellation

From Fig. 3.10, the symbol s_4 is correctly detected only if r falls in the horizontal pink region as indicated by the following expression

$$p(c|s_4)=p\left(\Re_r<-2d\sqrt{\frac{\xi_s}{\xi_{av}}}\middle|s_4\right)p\left(\Im_r\geq 0,\Im_r<2d\sqrt{\frac{\xi_s}{\xi_{av}}}\middle|s_4\right). \quad (3.81)$$

After substituting part of Eq (3.73) and part of Eq (3.78) into Eq (3.81), this results in

$$p(c|s_4) = \left[1-\frac{1}{2}\text{erfc}\left(d\sqrt{\frac{\xi_s}{2\sigma_x^2\xi_{av}}}\right)\right]\left[1-\text{erfc}\left(d\sqrt{\frac{\xi_s}{2\sigma_y^2\xi_{av}}}\right)\right]$$

$$= \left[1-\frac{1}{2}\text{erfc}\left(d\sqrt{\frac{\xi_s}{N_0\xi_{av}}}\right)\right]\left[1-\text{erfc}\left(d\sqrt{\frac{4\sin^2(-\frac{\varphi}{2})\xi_s}{\xi_{av}N_o}}\right)\right]. \quad (3.82)$$

After using Eq (3.63), the probability of symbol s_4 being detected incorrectly is

$$\begin{aligned} p(e|s_4) &= 1-p(c|s_4) \\ &= \frac{2l+p-p\cdot l}{2}. \end{aligned} \quad (3.83)$$

In addition, it can be shown that $p(e|s_4) = p(e|s_1) = p(e|s_2) = p(e|s_7) = p(e|s_8) = p(e|s_{11}) = p(e|s_{13}) = p(e|s_{14})$. The subsequent bit error rate probability when symbol s_4 is incorrectly detected can be written as

$$\begin{aligned} p(e|b_4) &= 1-\left[1-\frac{1}{2k}\text{erfc}\left(d\sqrt{\frac{kE_b}{\xi_{av}N_0}}\right)\right]\left[1-\frac{1}{k}\text{erfc}\left(d\sqrt{\frac{4k\sin^2(-\frac{\varphi}{2})E_b}{\xi_{av}N_o}}\right)\right] \\ &= \frac{2k\cdot\ell+\wp\cdot k-\wp\cdot\ell}{2k^2}. \end{aligned} \quad (3.84)$$

Similarly it can be shown that $p(e|b_4) = p(e|b_1) = p(e|b_2) = p(e|b_7) = p(e|b_8) = p(e|b_{11}) = p(e|b_{13}) = p(e|b_{14})$.

3.4.3.4 Combination of all symbols

From Eq (3.75), Eq (3.76), Eq (3.79), Eq (3.80), Eq (3.83) and Eq (3.84), assuming that all the symbols are equally probable (4 centre symbols, 4 corner symbols and 8 edge symbols), the SER and BER expressions for a 16-QAM constellation are given as

$$\begin{aligned} SER_{16QAM} &= \frac{4}{16}\left(\frac{l+p-p\cdot l}{1}\right)+\frac{4}{16}\left(\frac{2l+2p-p\cdot l}{4}\right)+\frac{8}{16}\left(\frac{2l+p-p\cdot l}{2}\right) \\ &= \left(\frac{14\cdot l+10p-9p\cdot l}{16}\right) \end{aligned} \quad (3.85)$$

and

$$BER_{16QAM} = \frac{4}{16}\left(\frac{k\cdot\ell+\wp\cdot k-\wp\cdot\ell}{k^2}\right)+\frac{4}{16}\left(\frac{2k\cdot\ell+2\wp\cdot k-\wp\cdot\ell}{4k^2}\right)+\frac{8}{16}\left(\frac{2k\cdot\ell+\wp\cdot k-\wp\cdot\ell}{2k^2}\right) = \frac{1}{16}\left(\frac{14k\cdot\ell+10\wp\cdot k-9\wp\cdot\ell}{k^2}\right). \quad (3.86)$$

3.4.3.5 A 64-QAM symbol and bit error rate derivation

A 64-QAM constellation, partially depicted in Fig. 3.11, is composed of four quadrants. Each quadrant contains 16 symbol points; consider one of these quadrants. Assuming that

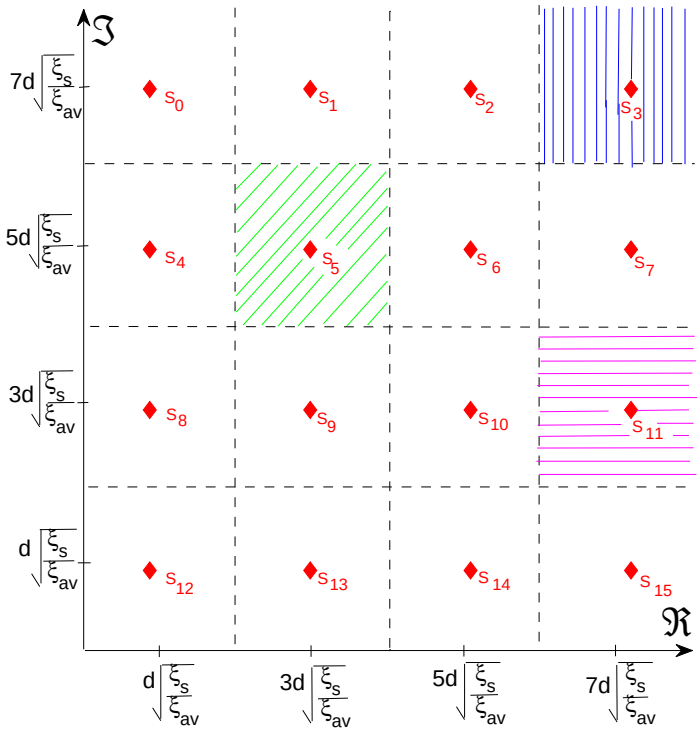

Figure 3.11: 64-QAM constellation

all the symbols of a 64-QAM constellation are equally probable (9 centre symbols in each of the 4 quadrants; 1 corner symbols in each of the 4 quadrants and 6 edge symbols in each

of the 4 quadrants), thereafter by using Eq (3.75), Eq (3.76), Eq (3.79), Eq (3.80), Eq (3.83) and Eq (3.84) the total probability of a symbol error and bit error are given as

$$\begin{aligned} SER_{64QAM} &= \frac{4\cdot 9}{64}\left(\frac{l+p-p\cdot l}{1}\right)+\frac{4\cdot 1}{64}\left(\frac{2l+2p-p\cdot l}{4}\right)+\frac{4\cdot 6}{64}\left(\frac{2l+p-p\cdot l}{2}\right) \\ &= \frac{1}{64}\left(\frac{62l+50p-49p\cdot l}{1}\right) \end{aligned} \tag{3.87}$$

and

$$\begin{aligned} BER_{64QAM} &= \frac{4\cdot 9}{64}\left(\frac{k\cdot \ell+\wp\cdot k-\wp\cdot \ell}{k^2}\right)+\frac{4\cdot 1}{64}\left(\frac{2k\cdot \ell+2\wp\cdot k-\wp\cdot \ell}{4k^2}\right)+ \\ &\quad \frac{4\cdot 6}{64}\left(\frac{2k\cdot \ell+\wp\cdot k-\wp\cdot \ell}{2k^2}\right) \\ &= \frac{1}{64}\left(\frac{62k\cdot \ell+50\wp\cdot k-49\wp\cdot \ell}{k^2}\right). \end{aligned} \tag{3.88}$$

This type of analysis can be extended further to investigate various other M-ary QAM constellations.

3.4.4 M-ary QAM symbol and bit error rate derivation

The previous sub-section has demonstrated the relationship between BER and SER. In this sub-section closed-form SER and BER expressions for M-ary QAM constellations are presented.

From the previous sub-sections, Table 3.3 and Table 3.4 present some of the results obtained. The remaining results were obtained after following a similar methodology. After studying these particular SER and BER expressions in Table 3.3 and Table 3.4, a particular relationship emerges which can be encapsulated by the following equations

$$SER_{EVEN} \approx \frac{l(M-2)+p\cdot(M-2\sqrt{M}+2)}{M}+\frac{p\cdot l(2\sqrt{M}-M-1)}{M}, \tag{3.89}$$

Table 3.3: Summarised SER QAM expressions

$QAM_{k=EVEN}$	**SER expressions**	$QAM_{k=ODD}$	**SER expressions**
4	$\frac{2l+2p-p\cdot l}{4}$	8	$\frac{6l+4p-3p\cdot l}{8}$
16	$\frac{14l+10p-9p\cdot l}{16}$	32	$\frac{30l+22p-21p\cdot l}{32}$
64	$\frac{62l+50p-49p\cdot l}{64}$	128	$\frac{126l+106p-105p\cdot l}{128}$
256	$\frac{254l+226p-225p\cdot l}{256}$	512	$\frac{510l+466p-465p\cdot l}{256}$

Table 3.4: Summarised BER QAM expressions

$QAM_{k=EVEN}$	**BER expressions**	$QAM_{k=ODD}$	**BER expressions**
4	$\frac{2k\cdot\ell+2\wp\cdot k-\wp\cdot\ell}{4k^2}$	8	$\frac{6k\cdot\ell+4\wp\cdot k-3\wp\cdot\ell}{8k^2}$
16	$\frac{14k\cdot\ell+10\wp\cdot k-9\wp\cdot\ell}{16k^2}$	32	$\frac{30k\cdot\ell+22\wp\cdot k-21\wp\cdot\ell}{32k^2}$
64	$\frac{62k\cdot\ell+50\wp\cdot k-49\wp\cdot\ell}{64k^2}$	128	$\frac{126k\cdot\ell+106\wp\cdot k-105\wp\cdot\ell}{128k^2}$
256	$\frac{254k\cdot\ell+226\wp\cdot k-225\wp\cdot\ell}{256k^2}$	512	$\frac{510k\cdot\ell+466\wp\cdot k-465\wp\cdot\ell}{256k^2}$

$$SER_{ODD} \approx \frac{\left(M-2-\left[\frac{3\sqrt{2}M-8\sqrt{M}}{2\sqrt{M}}\right]\right)p}{M} + \frac{(M-2)\cdot l-\left(M-3-\left[\frac{3\sqrt{2}M-8\sqrt{M}}{2\sqrt{M}}\right]\right)p\cdot l}{M}, \tag{3.90}$$

$$BER_{EVEN} \approx \frac{k\cdot\ell(M-2)+\wp\cdot k(M-2\sqrt{M}+2)}{M\cdot k^2}+\frac{\wp\cdot\ell(2\sqrt{M}-M-1)}{M\cdot k^2} \tag{3.91}$$

and

$$BER_{ODD} \approx \frac{\left(M-2-\left[\frac{3\sqrt{2}M-8\sqrt{M}}{2\sqrt{M}}\right]\right)\wp\cdot k}{M\cdot k^2} + \frac{(M-2)k\cdot\ell-\left(M-3-\left[\frac{3\sqrt{2}M-8\sqrt{M}}{2\sqrt{M}}\right]\right)\wp\cdot\ell}{M\cdot k^2}. \quad (3.92)$$

The subsequent expressions presented in Eq (3.89), Eq (3.90), Eq (3.91) and Eq (3.92) can be used to determine the SER and BER characteristics for any M-ary QAM OM-OFDM transmission.

3.4.5 M-ary PSK symbol and bit error rate derivation

In this sub-section an M-ary SER and BER expression for a PSK constellation is derived. In order to simplify the discussion the 16-PSK case will be discussed. This 16-PSK constellation, depicted in Fig. 3.12, can be adapted to include any M-ary PSK constellation.

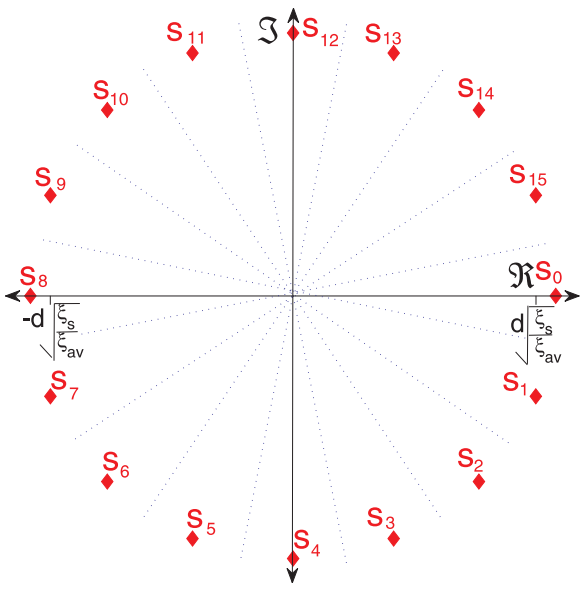

Figure 3.12: 16-PSK constellation

Consider symbol s_0, depicted in Fig. 3.12, on the real axis

$$s_0 = d\sqrt{\frac{\xi_s}{\xi_{av}}}. \tag{3.93}$$

The received symbol is $r = d\sqrt{\frac{\xi_s}{\xi_{av}}} + n$, where n is the AWGN noise. For a high SNR, the real part of the received signal, depicted in Fig. 3.13, should be correctly detected. As seen

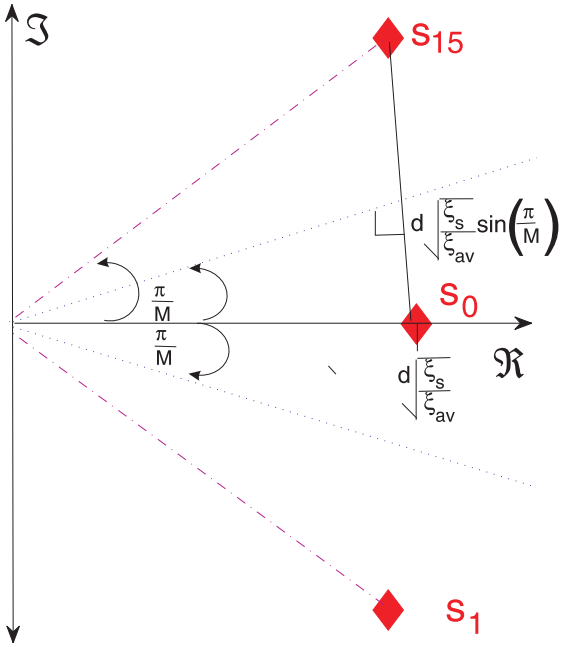

Figure 3.13: Distance between PSK constellation points

in Fig. 3.13, the symbol s_0 is incorrectly detected only if r falls outside the boundary region defined by the dotted blue lines. This may be expressed as

$$p(e|s_0) = p\left(\Im_r > d\sqrt{\frac{\xi_s}{\xi_{av}}}\sin\left(\frac{\pi}{M}\right)\middle| s_0\right) + p\left(\Im_r < -d\sqrt{\frac{\xi_s}{\xi_{av}}}\sin\left(\frac{\pi}{M}\right)\middle| s_0\right) \tag{3.94}$$

where

$$p\left(\Im_r > d\sqrt{\frac{\xi_s}{\xi_{av}}}\sin\left(\frac{\pi}{M}\right)\middle| s_0\right) = \frac{1}{\sqrt{2\pi}\sigma_y}\int_{d\sqrt{\frac{\xi_s}{\xi_{av}}}\sin(\frac{\pi}{M})}^{\infty} e^{\frac{-\Im_r{}^2}{2\sigma_y^2}}\, dr. \tag{3.95}$$

Let $u = \frac{-\Im_r}{\sqrt{2\sigma_y^2}}$, then

$$p\left(\Im_r > d\sqrt{\frac{\xi_s}{\xi_{av}}}\sin\left(\frac{\pi}{M}\right)\middle| s_0\right) = \frac{1}{\sqrt{\pi}}\int_{d\sqrt{\frac{\xi_s}{2\sigma_y\xi_{av}}}\sin(\frac{\pi}{M})}^{\infty} e^{-u^2}du$$
$$= \frac{1}{2}\text{erfc}\left(d\sqrt{\frac{\xi_s}{2\sigma_y\xi_{av}}}\sin\left(\frac{\pi}{M}\right)\right). \quad (3.96)$$

After substituting Eq (3.61) into Eq (3.96), this results in

$$p\left(\Im_r > d\sqrt{\frac{\xi_s}{\xi_{av}}}\sin\left(\frac{\pi}{M}\right)\middle| s_0\right) = \frac{1}{2}\text{erfc}\left(d\sqrt{\frac{4\xi_s}{N_0\xi_{av}}}\sin\left(\frac{\pi}{M}\right)\sin\left(\frac{-\varphi}{2}\right)\right). \quad (3.97)$$

The symbol s_0 is incorrectly detected if the imaginary component of the received real component is less than $-d\sqrt{\frac{\xi_s}{\xi_{av}}}\sin(\frac{\pi}{M})$. The probability of s_0 being incorrectly detected can be written as

$$p\left(\Im_r < -d\sqrt{\frac{\xi_s}{\xi_{av}}}\sin\left(\frac{\pi}{M}\right)\middle| s_0\right) = \frac{1}{\sqrt{\pi}}\int_{-\infty}^{-d\sqrt{\frac{\xi_s}{2\sigma_y\xi_{av}}}\sin(\frac{\pi}{M})} e^{-u^2}du$$
$$= \frac{1}{2}\text{erfc}\left(d\sqrt{\frac{4\xi_s}{N_0\xi_{av}}}\sin\left(\frac{\pi}{M}\right)\sin\left(\frac{-\varphi}{2}\right)\right). \quad (3.98)$$

The total conditional probability of an error, given that s_0 was transmitted, is

$$p(e|s_0) = \text{erfc}\left(d\sqrt{\frac{4\xi_s}{N_0\xi_{av}}}\sin\left(\frac{\pi}{M}\right)\sin\left(\frac{-\varphi}{2}\right)\right). \quad (3.99)$$

If it is assumed that each of M-PSK symbols are equally probable. The total symbol error probability for a M-PSK constellation is

$$SER_{PSK} = \text{erfc}\left(d\sqrt{\frac{4\xi_s}{N_0\xi_{av}}}\sin\left(\frac{\pi}{M}\right)\sin\left(\frac{-\varphi}{2}\right)\right). \quad (3.100)$$

For a Gray-coded constellation, when $(p(s_1|s_0)|p(s_{15}|s_0)) >> (p(s_2|s_0)|p(s_{14}|s_0))$ the sub-

sequent bit error rate can be written as

$$BER_{PSK} = \frac{1}{k}\text{erfc}\left(d\sqrt{\frac{4k\cdot E_b \sin^2\left(\frac{-\varphi}{2}\right)\sin^2\left(\frac{\pi}{M}\right)}{N_o}}\right). \tag{3.101}$$

The expressions presented in Eq (3.100) and Eq (3.101) can be used to determine the SER and BER characteristics for an M-ary PSK OM-OFDM transmission.

3.5 OM-OFDM PARAMETER SELECTION

In this section the manner in which the selection of the Ψ_{os}, ς and γ terms influences the derived 64-QAM BER expression, at a SNR=7 dB (E_b/N_o), will be investigated. Although this discussion may seem confined to this particular case (64-QAM, SNR=7 dB), it can be extended to include various other constellations. For the choice of Ψ_{os}, ς and γ terms, both Eq (3.44) and Table 3.2 (provided $0 \leq \varphi \leq \frac{\pi}{2}$) offer guidelines for these parameters. In order

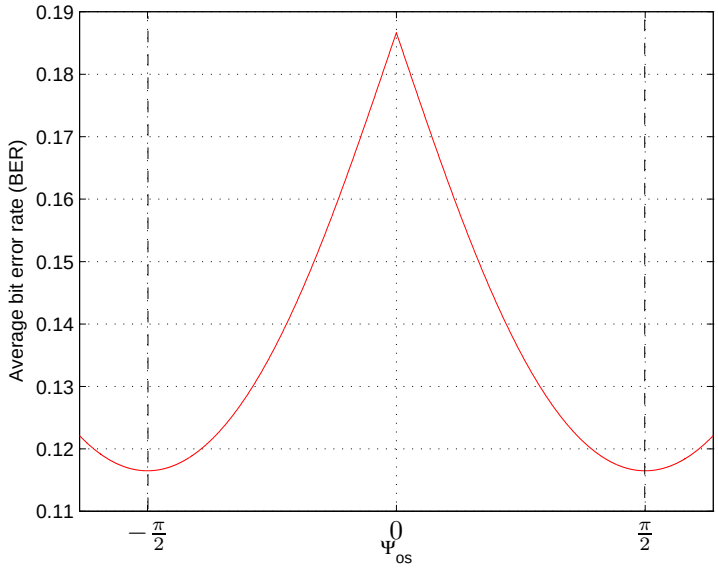

Figure 3.14: Ψ_{os} Parameter choice when $\gamma = 0.95$ and $\varsigma = 44000/16384$ in an AWGN channel for a 64-QAM constellation, with SNR=7 dB (E_b/N_o).

to obtain the relationship between BER and Ψ_{os}; the ς and γ terms are kept constant and the Ψ_{os} term is varied. As shown in Fig. 3.14, as Ψ_{os} approaches the limits ($\Psi_{os} = -\frac{\pi}{2}, \frac{\pi}{2}$),

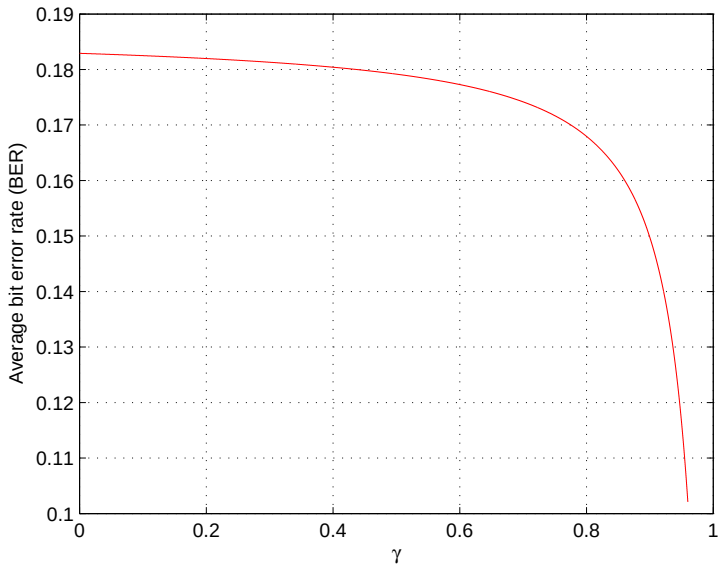

Figure 3.15: γ Parameter choice when $\Psi_{os} = 1.59$ and $\varsigma = 44000/16384$ in an AWGN channel for a 64-QAM constellation, with SNR=7 dB (E_b/N_o).

the noise components are lowered. As shown in Fig. 3.14, an increase in BER degradation is evident as the Ψ_{os} term moves away from these limits. It is also noted that as the ς term increases, the signal would lose resolution, which will affect the BER performance of the system.

Similarly in Fig. 3.15, in order to obtain the relationship between BER and γ; the Ψ_{os} and ς terms are kept constant and the γ term is varied. As shown in Fig. 3.15, as the γ term approaches 1, the noise decreases, since the PAPR is being sacrificed to obtain this BER performance improvement.

3.6 VALIDATION OF THE DERIVATION

Using these guidelines, the commonly used theoretically derived expressions needed to be validated. It should be noted that the theoretical expressions do not accept a $\gamma = 1$; if such a term arises, then $\varphi = 1$ (SER_{EVEN}, BER_{EVEN}), $\varphi = 1.5$ (SER_{ODD}, BER_{ODD}) and $\varphi = 1.23$ (SER_{PSK}, BER_{PSK}). These values simplify Eq (3.89), Eq (3.90), Eq (3.91), Eq (3.92), Eq (3.100) and Eq (3.101) into a SER and BER expression for an AWGN transmission.

By means of a simulation (the 2k or the 8k mode of the DVB-T2 standard [95]), offset modulated 4-QAM, 16-QAM and 64-QAM, as well as QPSK and 8-PSK Gray-coded signal constellations, were used to transmit data through an AWGN channel. The parameters used for the 4-QAM, 16-QAM, 64-QAM, QPSK and 8-PSK OM-OFDM transmission are given in Table 3.5, Table 3.6, Table 3.7, Table 3.8 and Table 3.9, respectively.

In these Tables the φ term is calculated by substituting the α, ς, Ψ_{os} and γ terms into the φ expression in Table 3.2. The specific terms (ς and Ψ_{os}) are chosen (as previously discussed in Section 3.5) such that they minimise the BER degradation, and the α term is obtained as indicated in Eq (3.18) and Eq (3.19).

In all these Tables the various parameters for a 7 dB - 13 dB PAPR range are presented. The γ term can be further varied, until an average PAPR in the range of 3 dB - 13 dB is reached. The lower bound (3 dB) is the ideal average PAPR [87] and the upper bound (12 dB or 13 dB) indicates the average PAPR of a traditional OFDM transmission [98] (since an attempt is made to reduce this PAPR).

Various BER comparisons between the theoretically derived and simulated OM-OFDM transmissions for various constellations are shown in Fig. 3.16, Fig. 3.17, Fig. 3.18, Fig. 3.19 and Fig. 3.20.

Table 3.5: Parameters for an 4-QAM OM-OFDM system ($\alpha = 0.036$)

PAPR	Ψ_{os}	ς	γ	φ
7 dB	1.5	10000/4096	0.9835	0.22
8 dB	1.5	10000/4096	0.9882	0.31
9 dB	1.5	10000/4096	0.992	0.4
10 dB	1.5	10000/4096	0.994	0.5
11 dB	1.5	10000/4096	0.996	0.7
12 dB	1.5	10000/4096	1	1

Table 3.6: Parameters for an 16-QAM OM-OFDM system($\alpha = 0.07408$)

PAPR	Ψ_{os}	ς	γ	φ
7 dB	1.5	10000/4096	0.963	0.205
8 dB	1.5	10000/4096	0.973	0.280
9 dB	1.5	10000/4096	0.98	0.378
10 dB	1.5	10000/4096	0.985	0.505
11 dB	1.5	10000/4096	0.988	0.631
12 dB	1.5	10000/4096	1	1.0

Table 3.7: Parameters for an 64-QAM OM-OFDM system ($\alpha = 0.27$)

PAPR	Ψ_{os}	ς	γ	φ
7 dB	1.596	44000/16384	0.86	0.2
8 dB	1.596	44000/16384	0.9	0.251
9 dB	1.596	44000/16384	0.925	0.34
10 dB	1.596	44000/16384	0.943	0.44
11 dB	1.596	44000/16384	0.962	0.53
12 dB	1.596	44000/16384	0.97	0.67
13 dB	1.596	44000/16384	1	1

Table 3.8: Parameters for QPSK OM-OFDM system ($\alpha = 0.027$)

PAPR	Ψ_{os}	ς	γ	φ
7 dB	1.5	10000/4096	0.98845	0.24
8 dB	1.5	10000/4096	0.992	0.3
9 dB	1.5	10000/4096	0.99418	0.4674
10 dB	1.5	10000/4096	0.996	0.55
11 dB	1.5	10000/4096	0.997	0.7
12 dB	1.5	10000/4096	1	1

Table 3.9: Parameters for 8-PSK OM-OFDM system ($\alpha = 0.027$)

PAPR	Ψ_{os}	ς	γ	φ
7 dB	1.5	10000/4096	0.9889	0.2485
8 dB	1.5	10000/4096	0.992	0.3
9 dB	1.5	10000/4096	0.9941	0.4674
10 dB	1.5	10000/4096	0.996	0.55
11 dB	1.5	10000/4096	0.997	0.7
12 dB	1.5	10000/4096	1	1

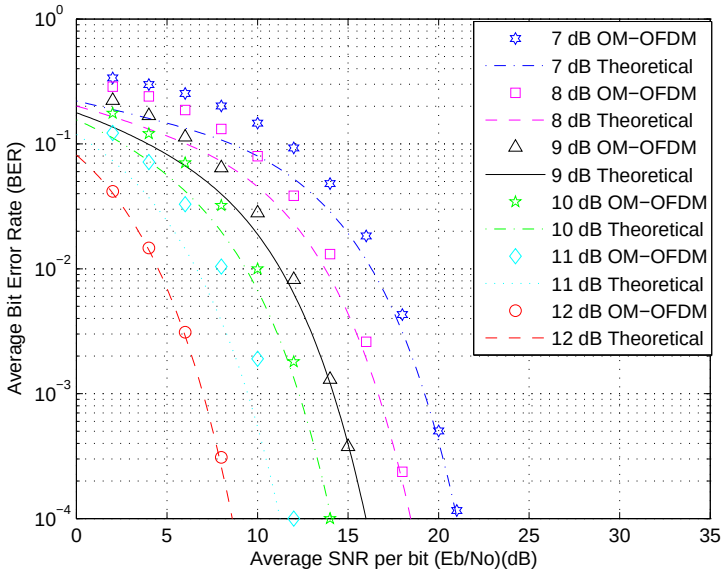

Figure 3.16: Theoretically derived (Eq (3.91)) and simulated BER comparisons for an OM-OFDM transmission in an AWGN channel for a 4-QAM constellation.

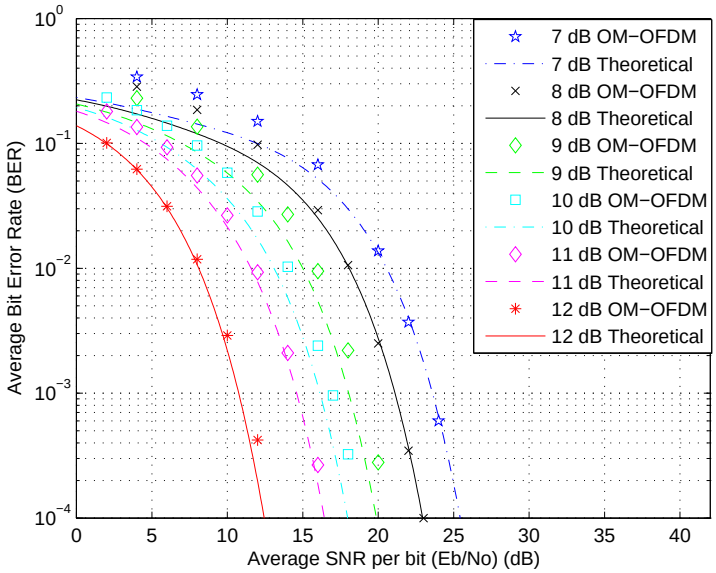

Figure 3.17: Theoretically derived (Eq (3.91)) and simulated BER comparisons for an OM-OFDM transmission in an AWGN channel for a 16-QAM constellation.

From this comparison, it is seen that the theoretically predicted results (Eq (3.91) and Eq (3.101)) and the simulated results correlate reasonably well, thus validating the theoretically derived expression. The slight difference between the simulated and theoretical results is due to the fact that the theoretical analysis does not take into account certain errors (e.g.

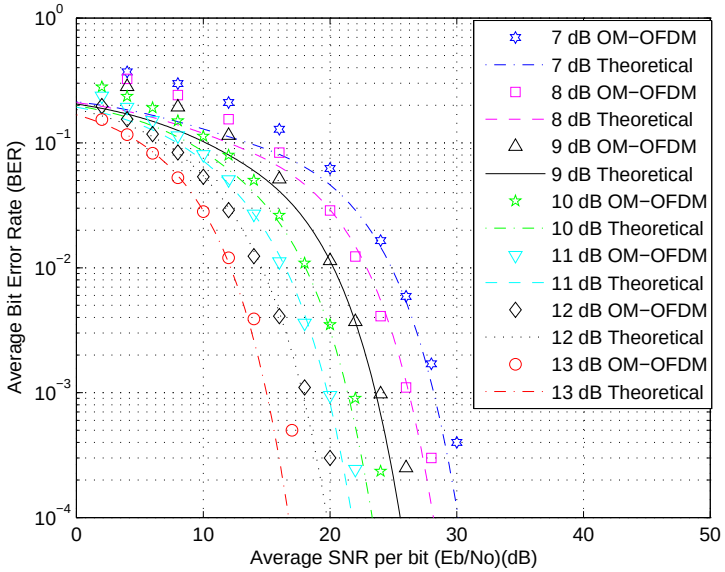

Figure 3.18: Theoretically derived (Eq (3.91)) and simulated BER comparisons for an OM-OFDM transmission in an AWGN channel for a 64-QAM constellation.

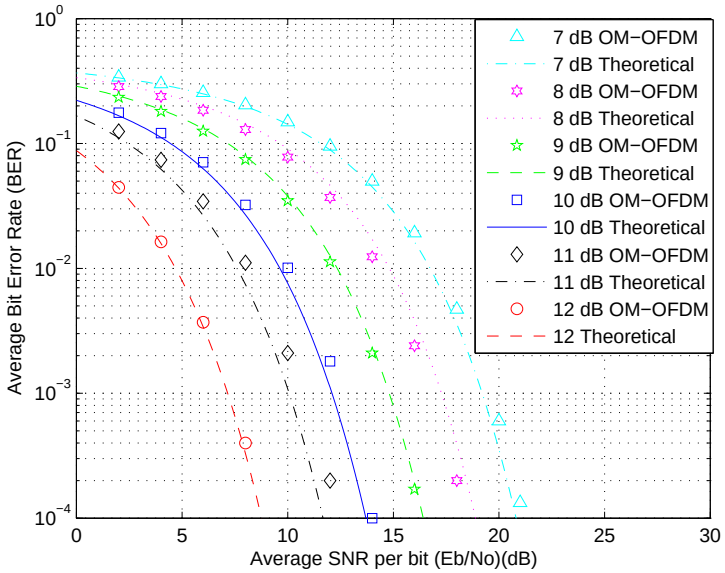

Figure 3.19: Theoretically derived (Eq (3.101)) and simulated BER comparisons for an OM-OFDM transmission in an AWGN channel for a QPSK constellation.

filter effects and quantisation effects, amongst others). Furthermore, Fig. 3.21, Fig. 3.22, Fig. 3.23, Fig. 3.24 and Fig. 3.25 depict the complementary cumulative distribution function for a 4-QAM, 16-QAM, 64-QAM, QPSK and 8-PSK OM-OFDM transmission, respectively.

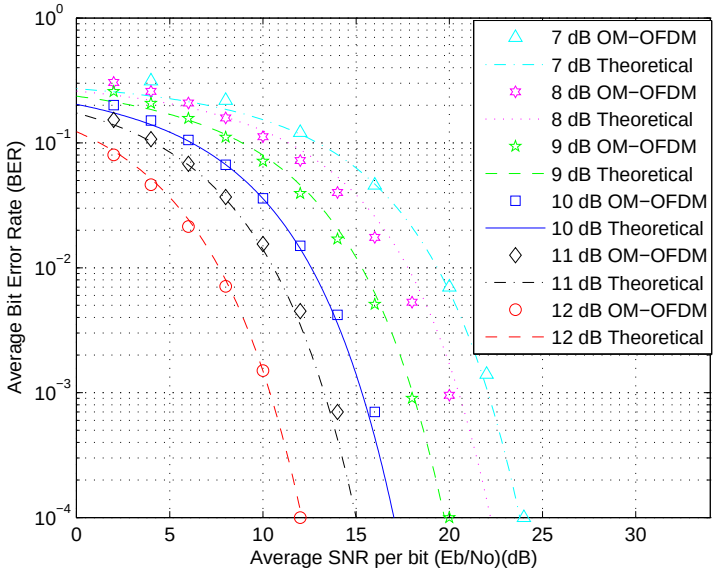

Figure 3.20: Theoretically derived (Eq (3.101)) and simulated BER comparisons for an OM-OFDM transmission in an AWGN channel for an 8-PSK constellation.

This CCDF graph can be interpreted as the probability of the various transmissions having a PAPR value above a certain threshold ($PAPR_o$). In the next section a decision metric is presented, which will later be used to determine the optimum OM-OFDM operating point.

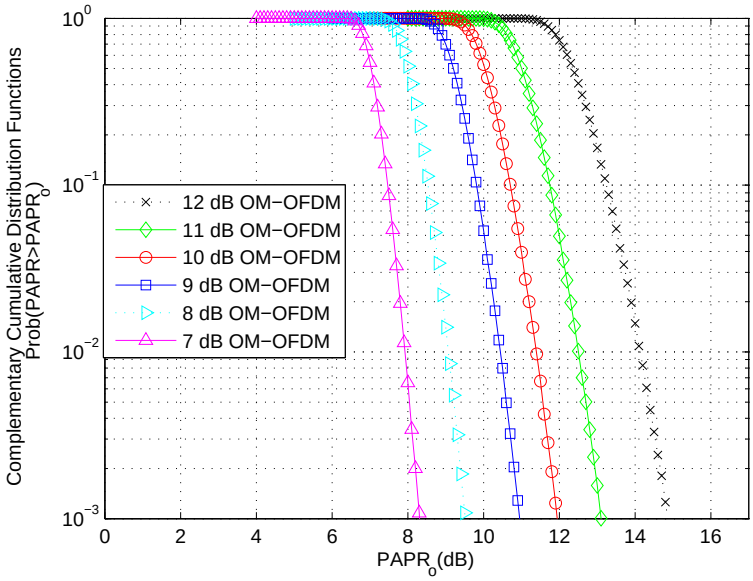

Figure 3.21: Complementary cumulative distribution functions for a 4-QAM constellation.

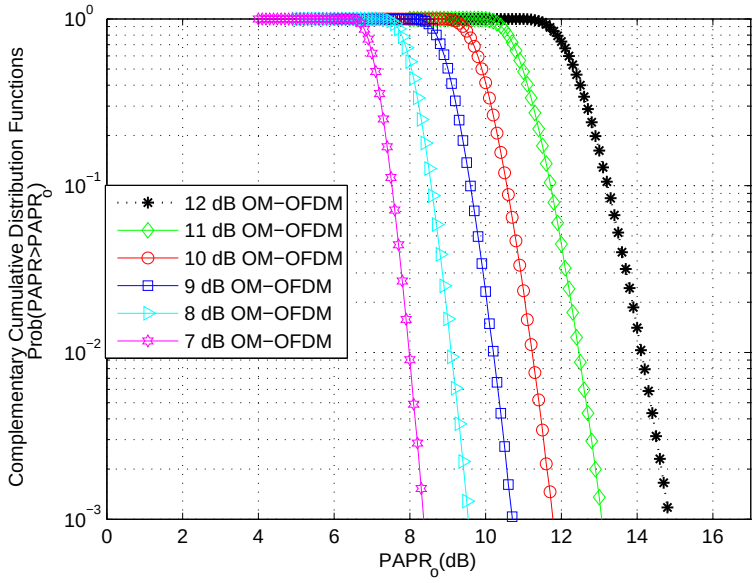

Figure 3.22: Complementary cumulative distribution functions for a 16-QAM constellation.

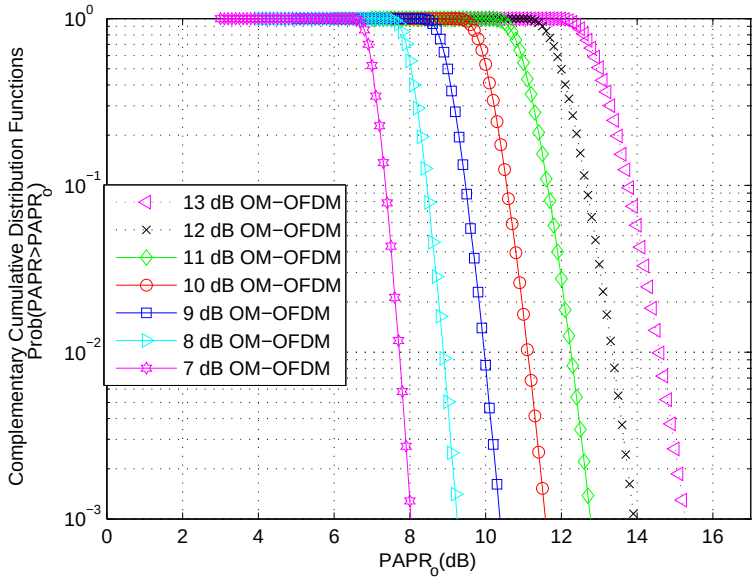

Figure 3.23: Complementary cumulative distribution functions for a 64-QAM constellation.

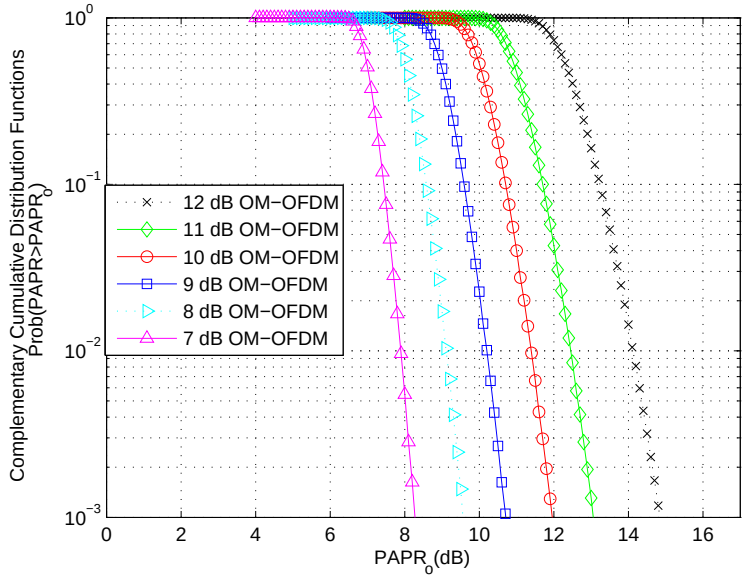

Figure 3.24: Complementary cumulative distribution functions for a QPSK constellation.

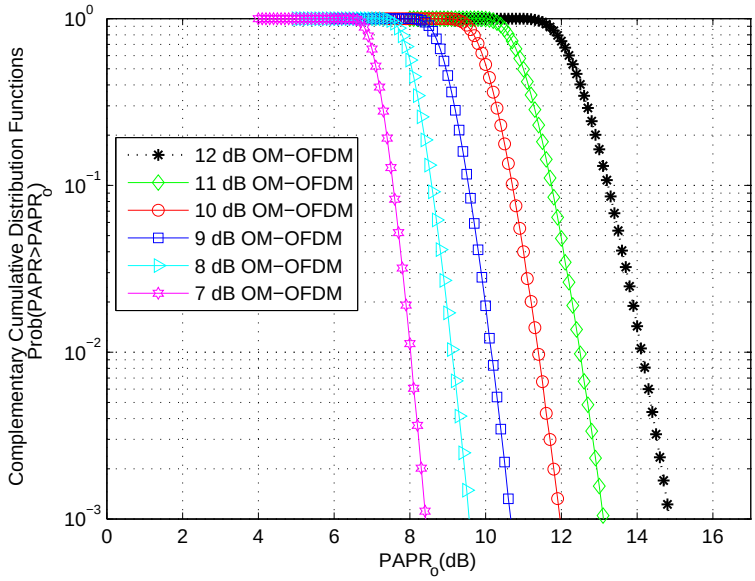

Figure 3.25: Complementary cumulative distribution functions for an 8-PSK constellation.

3.7 DECISION METRIC

The conventional metric used to describe a communication system is BER, which is usually a function of $\frac{E_b}{N_o}$. The relationship between energy per bit E_b, average received power $\overline{P_r}$ and data rate R_b is given by [99]

$$E_b \quad (joules/bit) \quad = \quad \frac{\overline{P_r} \quad (joules/s)}{R_b \quad (bits/s)}. \tag{3.102}$$

The E_b only takes into account the received energy per bit and offers no indication of the actual total energy required (e.g. dc power consumption of the amplifier) for transmission of an information bit. To obtain an indication of this, consider the instantaneous power-added efficiency (PAE) of the amplifier given by

$$P_{ae} \quad = \quad \frac{P_{rf}(t) - P_{in}(t)}{P_{dc}(t)} \tag{3.103}$$

where $P_{dc}(t)$ is the dc power supplied to the amplifier, P_{in} and P_{rf} are the input and output RF powers of the amplifier, respectively. The average total power $\overline{P_t}$ consumed by an amplifier, after using Eq (3.103), can be written as

$$\begin{aligned} \overline{P_t} &= \overline{P_{dc}} + \overline{P_{in}} \\ &= \overline{P_{rf}}\left(1 + \frac{\overline{P_{dc}}(1-\overline{P_{ae}})}{\overline{P_{rf}}}\right) \\ &= \overline{P_{rf}}(1+w) \end{aligned} \tag{3.104}$$

where $\overline{X}$ denotes the average power of X and w refers to the fractional average power not converted to RF power. The total energy per bit E_t for a given BER and N_o can be written as

$$\begin{aligned} E_t &= \frac{\overline{P_t}}{R_b} \\ &= \frac{\overline{P_r}(1+w)}{R_b} \\ &= E_b + E_w. \end{aligned} \tag{3.105}$$

In Eq (3.105), $\overline{P_r}$ is the average received power and $\overline{P_{rf}} = \overline{P_r}$. In addition E_w is the wasted energy per bit due to the inefficient power amplifier utilisation. As the input drive level increases, the E_w decreases. Increasing the input drive level improves efficiency; however, if an optimum back-off is not maintained, this distorts the signal waveform, which results in a BER trade-off. Another metric used to describe spectral efficiency is

$$\frac{R_b}{W} \quad (bits/s/Hz), \tag{3.106}$$

where R_b is the data rate and W refers to the bandwidth occupancy. Liang et al. [99] have proposed a decision metric (D), which combines two metrics and is given by

$$D = \frac{E_t}{N_o} \cdot \frac{W}{R_b}, \tag{3.107}$$

Unlike traditional approaches, which only take into account the received energy per bit (E_b) and often ignore the total energy consumption (e.g. dc power consumption of the amplifier), here, E_t incorporates the total energy per bit and as discussed (Eq (3.105)) can be written as

$$E_t = E_b + E_w, \tag{3.108}$$

where, E_w is the wasted energy per bit due to inefficient power amplifier utilisation. In order to determine E_t, the PAE of the amplifier which is to be used, is required. Liang et al. [99] have used this metric to investigate the trade-offs between amplifier efficiency, amplifier distortion, signal bandwidth occupation, throughput and power consumption. The purpose of the decision metric was to investigate an optimum combination of these factors to minimise the energy required. This metric can be adapted to investigate whether the proposed OM-OFDM transmission has an optimum solution and whether a net gain exists for such a solution. This adaptation involves considering that typically during fair comparisons, identical throughput and bandwidth occupancies are used, thus $\frac{W}{R_b}$ remains constant and the metric simplifies to

$$D \propto \frac{E_t}{N_o}. \tag{3.109}$$

This metric can also be utilised to compare various PAPR methods in the field. In addition, if both the BER compromise and the efficiency effects of the PAPR reduction, when using OM-OFDM, are considered, an optimum total energy per bit and PAPR value may be found. Thus an optimal solution for an OM-OFDM transmission may be obtained. In the rest of this thesis this metric is applied to various amplifiers.

3.8 CONCLUDING REMARKS

In this chapter a novel method, called offset modulation, is proposed to control the PAPR of an OFDM signal. The theoretical bandwidth occupancy of the proposed offset modulated signal is derived. Using these bandwidth occupancy results, a closed-form theoretical BER expression for an offset modulated transmission is derived and validated. A newly applied power performance decision metric is also introduced, which can be utilised to compare various PAPR methods.